

# RESEARCH MEMORANDUM

A COMPARISON OF SEVERAL SYSTEMS OF BOUNDARY-LAYER  
REMOVAL AHEAD OF A TYPICAL CONICAL  
EXTERNAL-COMPRESSION SIDE INLET  
AT MACH NUMBERS OF 1.88 AND 2.93

By Thomas G. Piercy and Harry W. Johnson

Lewis Flight Propulsion Laboratory  
Cleveland, Ohio

NATIONAL ADVISORY COMMITTEE  
FOR AERONAUTICS  
WASHINGTON

September 4, 1953  
Declassified July 28, 1958

THE UNIVERSITY OF CHICAGO

DEPARTMENT OF CHEMISTRY

LABORATORY OF ORGANIC CHEMISTRY

REPORT OF RESEARCH

BY

ROBERT M. WAYNE

1953

RESEARCH ASSISTANT

ADVISOR

ROBERT M. WAYNE

1953

CHICAGO, ILLINOIS

NATIONAL ADVISORY COMMITTEE FOR AERONAUTICS

RESEARCH MEMORANDUM

A COMPARISON OF SEVERAL SYSTEMS OF BOUNDARY-LAYER REMOVAL AHEAD OF  
A TYPICAL CONICAL EXTERNAL-COMPRESSION SIDE INLET AT MACH  
NUMBERS OF 1.88 AND 2.93

By Thomas G. Piercy and Harry W. Johnson

SUMMARY

An experimental investigation was conducted at Mach numbers of 1.88 and 2.93 to determine the performance characteristics of a conical external-compression side inlet model utilizing a swept-leading-edge boundary-layer-removal scoop. Two alternative boundary-layer-removal systems were also investigated wherein removal was accomplished by means of a  $62^{\circ} 6'$  deflection wedge, which replaced the ducting of the swept scoop, and by cowl-lip scoops. Comparisons are made with the performance of the inlet utilizing the ram scoop (straight leading edge with enclosed sides) and other removal systems previously reported.

With maximum removal of the boundary layer, the inlets with straight and swept-leading-edge scoops were found to give essentially the same total-pressure recovery. At Mach 1.88 the maximum total-pressure recovery was approximately 89 percent. At Mach 2.93 the maximum total-pressure recovery of all systems of removal investigated herein was approximately 49 percent, although 51.5 percent was achieved in previous tests using the ram-scoop removal system. When the mass flow captured by the boundary-layer scoop was reduced, the swept-scoop inlet was found to exhibit approximately the same large adverse effect on inlet pressure recovery and stability as was previously observed with the straight ram scoop.

The deflection wedge and the cowl-lip scoop removal systems were found to give total-pressure recoveries comparable with those of the ducted scoops when the boundary-layer-removal system was sufficiently large in comparison with the boundary-layer thickness. At equivalent pressure recovery the cowl-lip scoop spilled the least amount of air and indicated a total projected frontal area of inlet plus scoop as small as or smaller than the inlet with conventional scoop or wedge removal systems.

## INTRODUCTION

The use of the ram-type boundary-layer scoop (straight leading edge with enclosed sides) as a means of removing the boundary layer ahead of conical external-compression side inlet configurations at Mach numbers of 1.88 and 2.93 has been reported in references 1 and 2, respectively. The inlet for these tests was mounted on a flat plate at zero angle of attack and yaw with respect to the local free stream. It was observed that, with sufficient removal of the boundary layer ahead of the inlet, total-pressure recoveries comparable with those of nose inlets could be obtained at Mach 1.88; while at Mach 2.93 the total-pressure recovery was slightly lower than that obtained with a nose inlet for the case considered. Some recent investigations of other side inlet configurations using boundary-layer-removal scoops installed on the fuselage of a proposed supersonic airplane are reported in references 3 to 5.

The investigations reported in references 1 and 2 with the ram-scoop removal system have indicated that while the inlet performance was acceptable with sufficient removal of the boundary layer, reduction of the amount of boundary-layer removal severely reduced the inlet total-pressure recovery. If the reduction in removal occurred through a reduction in the boundary-layer-scoop mass flow with resultant spillage into the inlet, an additional adverse effect of unstable operation was encountered.

In reference 1 several alternative systems of boundary-layer removal wherein the boundary layer was diverted around the inlet were investigated briefly. For those tests the boundary layer was simply allowed to spill to the sides around the inlet, either beneath the splitter plate separating the inlet and boundary-layer flows or through inlet-cowl slots. Inlet total-pressure recovery for all variations of boundary-layer removal investigated showed improvements over that obtained with the ducted scoop when no boundary layer was allowed to enter the duct (i.e., low scoop mass-flow ratio). The swept-leading-edge splitter plate with complete blockage of the flow downstream of the inlet and beneath the splitter plate was the most effective of the variations investigated. This configuration successfully diverted the boundary layer around the inlet.

For the designer who wishes to use the air obtained from boundary-layer removal for cooling or as a source of secondary air in ejector designs, the swept-leading-edge boundary-layer scoop with ducting therefore appeared promising; pressure recovery obtained with maximum removal of the boundary layer should be equivalent to that previously obtained using a ram scoop, and the inlet pressure recovery should be less sensitive to boundary-layer scoop mass flow because of the ability of the

boundary layer to spill to the sides of the inlet rather than over the splitter plate and into the inlet.

In the present investigation the performance of the inlet with the swept scoop was determined at Mach numbers of 1.88 and 2.93 at the NACA Lewis laboratory and compared with the inlet performance obtained using the ram scoop of references 1 and 2. In addition, wedges beneath the splitter plate and cowl-lip scoops were investigated and compared with other methods of boundary-layer removal.

SYMBOLS

The following symbols are used in this report:

- $C_p$  static-pressure coefficient, defined by  $\left(\frac{P_w - P_0}{q_0}\right)$
- $C_{d_p}$  pressure drag coefficient, defined by  $\frac{1}{z_{max}} \int_0^{z_{max}} c_p dz$
- $h$  height of boundary-layer-removal system above flat plate
- $h/\delta$  dimensionless boundary-layer scoop height parameter
- $L$  plate length, measured from leading edge to spike tip
- $L/R$  dimensionless plate length parameter
- $M$  Mach number
- $m$  mass flow
- $N$  boundary-layer profile parameter, based on  $V/V_0 = (y/\delta)^{1/N}$
- $P$  total pressure
- $p$  static pressure
- $q$  free-stream dynamic pressure,  $q_0 = \frac{\gamma}{2} p_0 M_0^2$
- $R$  inlet radius, 1.5 in.
- $V/V_0$  ratio of velocity in boundary layer to free-stream velocity
- $y$  normal distance above plate

2944

$z$	lateral distance from center line of inlet measured parallel to plate
$\gamma$	ratio of specific heats = 1.4
$\delta$	boundary-layer thickness, distance from flat plate surface to point in boundary layer where velocity is equal to 0.99 free-stream velocity
$\delta/R$	dimensionless boundary-layer thickness parameter
$\delta^*/\theta$	boundary-layer form factor, quotient of boundary-layer displacement and momentum thicknesses

## Subscripts:

D	inlet
max	maximum
s	boundary-layer scoop
w	wedge
0	free stream
1	conditions 1/2 inch upstream of spike tip
2	conditions at exit of diffuser or boundary-layer scoop

## APPARATUS AND PROCEDURE

## Boundary-Layer-Removal Systems

The side inlet configurations utilizing ram-type scoops investigated at Mach numbers of 1.88 and 2.93 have been described in references 1 and 2, respectively. The inlet in each case was half-conical, with external compression provided by cone half-angles of  $25^\circ$  and  $30^\circ$  for Mach numbers of 1.88 and 2.93, respectively. The inlets were mounted on a flat plate, and the boundary layer which developed on the plate was removed with scoops having leading edges normal to the flow. The inlets were at zero angle of attack and yaw with respect to the local free stream. For the majority of the present tests the boundary-layer-removal system was modified as follows (see fig. 1(a)):

(a) The splitter plate dividing the flow for the inlet and boundary-layer scoop was swept from the spike tip to the lip of the inlet. This resulted in sweep angles of  $42^{\circ} 36'$  and  $38^{\circ} 58'$  for the configurations of Mach numbers 1.88 and 2.93, respectively.

(b) The swept splitter plate was beveled on the lower side at approximately  $9.5^{\circ}$  in the streamwise plane. The flat plate upon which the initial boundary layer was built up was machined out directly beneath the splitter plate, so that for zero removal of the boundary layer ( $h = 0$ ), the splitter plate could become flush with the main plate. The beveling of the splitter plate and the machining of the main plate were performed to lessen the possibility of choking beneath the splitter plate at small values of  $h$ . (Details of the swept-scoop configuration may be seen in photographs of a related model in fig 12.)

In addition to the removal of the boundary layer through scoops, two alternative systems of boundary-layer removal were investigated. The first of these employed a wedge beneath the splitter plate to divert the boundary layer. This wedge was instrumented with static-pressure taps to provide data for determination of the pressure drag incurred with this system of removal. The wedge removal configuration is shown schematically in figure 1(b), while a photograph of the model installed in the 18- by 18-inch Mach 3.05 tunnel is included in figure 1(c). The wedge tip was located at the apex of the conical spike with the wedge swept back at as small an included angle ( $62^{\circ} 6'$ ) as the model would permit.

The second alternative system of boundary-layer removal was an adaptation of cowl slots introduced in reference 6. "Cowl-lip" scoops were provided to forcibly spill the boundary layer through the cowl slots. This was accomplished by a continuation of the spike centerbody to the cowl and by providing a splitter plate inside the lip to divide the boundary-layer scoop and main inlet flows. The cowl-lip scoop configuration is shown schematically in figure 1(d); a photograph of the model installed in the 18- by 18-inch Mach 1.91 tunnel is included in figure 1(e).

### Instrumentation

For the boundary-layer-removal systems involving ducting, a system of rotameters was used to measure and control the mass flow through the boundary-layer scoop, as described in references 1 and 2. The flow captured by the scoop was returned to the tunnel test section. Total pressures in the boundary-layer duct were measured with a 17-tube rake.

For the tests at Mach 1.88 the flow properties following diffusion were determined with the rake shown in figure 2. The rake consisted of 13 pitot-static tubes each of which (with the exception of the center tube) was located at the centroid of equal areas. The rake was located approximately 2 diffuser exit diameters downstream of the end of the diffuser section. Mass flow through the inlet was remotely controlled with a butterfly valve and was measured with a standard A.S.M.E. 4-inch orifice, as described in reference 1.

For the tests at Mach 2.93, inlet mass flow was controlled with a movable exit plug, and flow characteristics following diffusion were determined with a rake consisting of 41 total-pressure tubes, 4 static-pressure tubes, and 4 wall static orifices. This instrumentation was the same as that described in reference 2.

#### Boundary-Layer Data

The boundary layer 1/2-inch upstream of the spike tip was determined from pressure measurements as described in references 1 and 2 for a plate length parameter  $L/R$  of 9.67. The initial defects in mass flow and total pressure due to the presence of the boundary layer are reproduced in figure 3. Carborundum dust near the leading edge of the plate developed turbulent boundary-layer profiles with the characteristics presented in the following table:

$M_0$	$L/R$	$\delta^*/\theta$	$\delta/R$	$N$
1.88	9.67	2.85	0.150	7
2.93	9.67	5.05	.160	7

The power profile parameter  $N$  was determined using the calculated values of  $\delta^*/\theta$  from reference 7.

#### Test Conditions and Variables

Test-section total temperature was held at 150° F, while the total pressure was essentially atmospheric. This resulted in test-section Reynolds numbers of the order of  $3.24 \times 10^6$  and  $1.75 \times 10^6$  per foot for test Mach numbers of 1.88 and 2.93, respectively. The dew point was maintained in the range -20° to -5° F to ensure negligible water condensation effects.

For the configurations employing swept-leading-edge boundary-layer scoops, the boundary-layer scoop height  $h$  was varied from zero to a



value greater than the boundary-layer thickness. At each scoop height the inlet mass flow was varied from the supercritical value to well within the inlet instability region, and the boundary-layer scoop flow was varied from the maximum attainable to zero. Inlet total-pressure recovery was obtained as a function of inlet mass flow, scoop mass flow, and the height of the boundary-layer scoop.

For the wedge configurations the original flat plate (i.e., without the indentation beneath the splitter plate) was used. Systematic variation of the amount of boundary-layer removal was obtained by varying the height of the wedge. Inlet pressure recovery and mass flow were determined as described previously.

For the cowl-lip scoop configurations the nonindented flat plate was also used. The height of the scoop was varied in steps to obtain the effect of various amounts of boundary-layer removal on the inlet pressure recovery and mass flow.

Pressures were recorded photographically on multimanometer boards. Schlieren pictures of the flow in the vicinity of the inlet were made during steady and unsteady conditions. Pressures and mass flows presented during unstable operation represent, as nearly as possible, average values.

#### Mass-Flow and Total-Pressure Referencing

As described in references 1 and 2, the mass flow and total-pressure recovery of the side inlet with scoop-type removal were referenced to conditions 1/2 inch upstream of the spike tip. The reference total pressure  $P_{1,D}$  represents an area-weighted pressure composed of free-stream and the lower energy boundary-layer flow in the stream tube of the projected inlet area. Similarly, the mass flow  $m_{1,D}$  represents the area-weighted mass flow in the stream tube of the projected inlet area decreased by approximately 7 percent design spillage. Total pressure and mass flow expressed as ratios of the free-stream values for the inlet and scoop are reproduced in figure 3 as functions of the boundary-layer scoop height parameter  $h/\delta$ . These curves permit the data presented to be referenced to free-stream conditions if desired.

## DISCUSSION OF RESULTS

## Swept-Scoop Inlet

For each value of the swept-scoop height investigated, the boundary-layer scoop mass flow was varied from the maximum attainable to zero for several values of the diffuser exit Mach number. The data are presented in figures 4 and 5 for Mach numbers of 1.88 and 2.93, respectively, for several values of  $h/\delta$ . Inlet total-pressure recovery  $P_{2,D}/P_{1,D}$  is plotted as a function of inlet mass-flow ratio  $m_D/m_{1,D}$ , with the scoop mass-flow ratio  $m_s/m_{s,max}$  and diffuser exit Mach number  $M_2$  as parameters. Dashed lines represent unstable operation. (It should be noted that  $m_{1,D}$  incorporates approximately 7 percent spillage.) It is immediately evident from these plots that, contrary to expectations, the inlet was quite sensitive to boundary-layer scoop mass flow. A comparison of these plots with similar data in references 1 and 2 shows only a very slight improvement in this respect. However, with supercritical inlet operation, it was noted that inlet stability was slightly less sensitive to reduced scoop mass flow using the swept scoop as compared with the ram scoop.

Swept boundary-layer scoop at Mach 1.88. - At Mach 1.88 (fig. 4) peak total-pressure recovery occurred at smaller inlet mass flow than was noted for the ram scoop. Visual evidence of the stable subcritical operation possible with the swept scoop is shown in figure 6, which has been retouched slightly for clarity. For both ram and swept scoops it was noted that at the larger values of  $h/\delta$  investigated peak pressure recovery was attained with slightly reduced scoop mass flow.

With supercritical inlet operation some indications of the desired reduction of sensitivity of the inlet to the scoop mass flow were noted, since the scoop mass flow could be reduced as much as 25 percent with very little reduction of inlet pressure recovery or mass flow. Insight into this reduction in sensitivity may be gained by referring to figure 6(d). Even with maximum scoop mass flow, a partially expelled shock system was noted beneath the splitter plate. For a limited range of scoop mass-flow ratios prior to the onset of scoop instability, the resultant spillage was able to pass around the inlet with the swept splitter plate rather than into the inlet.

Swept boundary-layer scoop at Mach 2.93. - At Mach 2.93 the inlet mass flow at peak pressure recovery was essentially the same as that obtained with the ram scoop. Peak pressure was generally accompanied by a small amount of inlet instability. Some of the schlieren photographs of the peak pressure condition in figure 7 show a slight fuzziness of the lip shock, indicating the magnitude of the instability. No bow shock was evident, as with previous results using the ram scoop. Peak pressure

was again attained at slightly reduced scoop mass flow for  $h/\delta$  greater than 1.0. Some reduction in inlet sensitivity to scoop mass flow was noted as for the lower Mach number.

Summary of swept scoop and comparison with ram scoop. - Summary plots of the side inlet performance with swept-scoop boundary-layer removal are presented in figures 8 and 9 for Mach numbers of 1.88 and 2.93, respectively. Peak total-pressure recovery is plotted as a function of boundary-layer scoop height parameter  $h/\delta$  and scoop mass-flow ratio  $m_s/m_{s,max}$ . Regions of inlet instability are represented by dashed curves. These results are similar to those previously reported for the ram scoop and show graphically the sensitivity of inlet pressure recovery to boundary-layer removal. The regions of inlet instability are essentially the same as those reported for the ram scoop.

In figures 10 and 11 comparisons are presented of the peak total pressure for the cases of maximum and zero removal of the boundary layer as a function  $h/\delta$  for the ram and swept scoops for the two Mach numbers considered. With maximum removal of the boundary layer ( $m_s/m_{s,max} = 1.0$ ), the two systems of removal gave essentially the same pressure recovery; at Mach 1.88 in figure 10 the peak total-pressure recovery is approximately 89 percent. The most significant difference in pressure recovery occurred at Mach 2.93 near  $h/\delta$  of 0.9; the peak total-pressure recovery with swept-scoop removal is 49.6 percent compared with 51.5 percent for the ram scoop. This discrepancy is not readily explained but may have resulted from the slight change in Reynolds number. With no boundary layer being taken into the scoop ( $m_s = 0$ ), some improvements in pressure recovery were observed using the swept-scoop configuration.

Visual flow observations. - During unstable operating conditions the shock patterns were found to vary with  $h/\delta$ , boundary-layer scoop mass flow, and degree of subcritical operation. These shock patterns were described fully in reference 2 and apply equally well for the swept-scoop configuration. One minor difference noted was that for subcritical operation with the swept scoop the shock disturbance was not propagated upstream to the end of the plate as it was with the ram scoop. It is believed that the ability of the boundary-layer scoop to spill around the sides of the inlet may be an important factor affecting this reduction in degree of shock instability.

An attempt to examine the flow inside the inlet was made by modifying the swept-scoop model used in the tests at Mach 1.88 by replacing the outer metal half-cylindrical section with a Plexiglas window. This required a modified external lip section, the first 1/2 inch of which was identical to the original section. Small thread tufts were mounted on one-half of the Plexiglas window, on the inlet centerbody, and along

the floor of the inlet between the centerbody and the window. In figure 12 the movement of the internal shock from well within the subsonic diffuser to peak pressure recovery is presented. As indicated in figure 12, separation occurred behind the internal shock, especially on the centerbody and on the floor of the inlet next to the centerbody. No separation was noted on the Plexiglas window except in the immediate vicinity of the shock, indicating a rapid reattachment on the surface subjected to the least boundary layer. It was observed that, at the peak pressure conditions for the larger values of  $h/\delta$ , reattachment of the boundary layer on the centerbody occurred sufficiently forward to be viewed through the Plexiglas window. This reattachment of the boundary layer on the centerbody was not observed at smaller values of  $h/\delta$ , substantiating the belief that the boundary layer entering the inlet tends to destabilize the internal flow. Inlet instability was characterized by a rapid fore and aft movement of all tufts, indicating an actual reversal of the flow. When the inlet was operating supercritically, decreasing the scoop mass flow until scoop instability occurred produced essentially the same results, with the oscillation of the tufts being most noticeable on the floor and on the centerbody.

#### Scoop Performance

Performance characteristics of the swept scoop are presented in figure 13. Scoop total pressure  $P_{2,s}/P_0$  is plotted as a function of the theoretical scoop mass-flow ratio  $m_s/m_{1,s}$  for several values of  $h/\delta$ . The theoretical mass flow which would be captured in the stream tube of the projected scoop if no spillage occurred is represented by  $m_{1,s}$ . A comparison of figures 13(a) and 13(b) with references 1 and 2, respectively, for the ram scoop indicates that the swept-scoop configuration spilled 15 to 20 percent more flow than the ram scoop at Mach 1.88, while 5 to 15 percent more was spilled at Mach 2.93. Peak scoop pressure recovery with the swept scoop is essentially the same as that obtained with the ram scoop at Mach 2.93; while at Mach 1.88, the swept scoop yields a slightly higher value. Included in figure 13 are the theoretical scoop total-pressure recovery data according to the method of reference 8. These data were obtained using a calculated power profile parameter  $N$  of 7, and correspond in the present notation to  $h/\delta$  of 1.0. Friction losses were not included. It is felt that most of the discrepancy between the theoretical and measured total pressures was due to the rather poor internal fairing of the boundary-layer duct, made necessary by the design requirement of variable scoop height as shown in figure 1(a); the wall friction is, of course, another contributing factor.

## Alternative Boundary-Layer-Removal Systems at Mach 1.88

In an attempt to provide the designer with information of the effectiveness of systems of boundary-layer removal in which the boundary layer is not taken into ducts but rather is diverted around the inlet beneath the splitter plate, several alternative systems of boundary-layer removal were attempted in reference 1 at Mach 1.88. These results are reproduced in figure 14. Shown for comparison are the ram-scoop data for maximum and zero boundary-layer removal. These latter two curves are slightly different from those presented in figure 10 because of the difference in the boundary-layer thickness parameter  $\delta/R$ .

The first variation attempted was that of removing the sides of the ram scoop to a point approximately one inlet radius downstream of the inlet lip. The boundary-layer duct was removed and replaced with a blunt deflector downstream of the inlet lip (fig. 4(b), ref. 1). The maximum total-pressure recovery, obtained at  $h/\delta$  of 1.0, was 7 percentage points lower than that obtained with complete removal through the scoop.

The second alternative was a simple modification of the first. The splitter plate dividing the inlet from the boundary layer was swept from the spike tip to the inlet lip (fig. 4(c), ref. 1). This arrangement worked especially well, giving a pressure recovery 3 percentage points below that obtained with the original scoop at  $h/\delta = 1.0$ . A third method employed cowl slots (fig. 4(d), ref. 1), allowing the low-energy air which accumulates in the corners to spill out of the inlet. This configuration was found to give essentially the same total pressure as the ram scoop at the larger values of  $h/\delta$ .

Another configuration investigated but not reported in reference 1 was a curved wedge installed beneath the splitter plate at  $h/\delta$  of 1.0. This wedge was approximately the same size as the wedge reported herein, but had concave rather than straight sides. This configuration gave a pressure recovery 5 percentage points below that obtained with the ram-scoop model.

Boundary-layer removal using  $62^\circ$  wedge. - To extend the data of alternative boundary-layer-removal systems, additional data were obtained on the wedge removal system. The model limited the minimum included wedge angle that could be used beneath the splitter plate to  $62^\circ 6'$ , with the tip of the wedge directly beneath the apex of the spike (figs. 1(b) and 1(c)). Wedges of various thicknesses were installed to give the variation of inlet pressure recovery with  $h/\delta$ , where  $h$  is defined as the thickness of the wedge plus the thickness of the splitter plate (0.032 in.). This definition of  $h$  is then equivalent to that used with scoop removal. Each wedge was instrumented

with static-pressure taps (shown schematically in fig. 20) in order that the pressure drag on the wedge could be determined. The resulting inlet pressure recovery - mass-flow characteristics as a function of  $h/\delta$  are presented in figures 15 and 16 for Mach numbers of 1.88 and 2.93, respectively. Inlet instability is again shown with dashed lines. At the lower Mach number, design supercritical spillage was obtained; whereas at Mach 2.93 additional spillage of the order of 5.5 percent was observed with the largest wedge heights. An oil-flow technique indicated a detached bow wave ahead of the wedge at both Mach numbers. The additional spillage at Mach 2.93 may perhaps be attributed to the effects of this detached wave on the boundary layer ahead of the inlet; it is not understood, however, why a similar effect was not observed at the lower Mach number.

Schlieren photographs of the peak pressure conditions are presented in figures 17 and 18. The detached bow wave ahead of the wedge at Mach 1.88 is indicated in figure 17, which has been retouched slightly for clarity. (It is not indicated in fig. 18 at Mach 2.93 because of the lack of sensitivity of the schlieren apparatus.) The standing bow wave ahead of the inlet at the peak pressure condition correlates the subcritical stability noted at the lower Mach number in figure 15.

During unstable inlet operation the shock disturbance was transmitted almost to the end of the plate for all values of  $h/\delta$  at the lower Mach number. At the higher Mach number the shock oscillation during buzz extended onto the plate at the lower values of  $h/\delta$ ; but for  $h/\delta$  of 1.133 and 1.655, the shock oscillation was restricted to the spike only. Typical examples of these buzz patterns are indicated in figures 19(a) and 19(b). Exposure time was approximately 1 microsecond. Figure 19(a) represents the shock pattern that extends upstream of the spike. Separation of the boundary layer behind the forward shock was observed. Figure 19(b) denotes a typical shock pattern on the spike. The normal shock moved from inside the lip to about one-half the distance between the lip and the spike during this unstable operation.

Wedge drag. - Wedge static-pressure distributions and orifice stations are presented in figure 20. The free-stream static pressure was determined with an orifice on the main plate located approximately 2.75 inches upstream of the spike tip. Each wedge was instrumented with one or more rows of static orifices with 4 orifices per row. The static-pressure coefficient at each orifice was determined from

$$C_p = \frac{2}{\gamma M_0^2} \left( \frac{p_w}{p_0} - 1 \right)$$

Inasmuch as the static pressure appeared to be a function of only the distance along the wedge (i.e., not a function of the vertical orifice location, except perhaps at the most upstream orifice station), the static pressures were averaged at each of the four orifice stations. The resulting static-pressure distributions along the wedge during supercritical inlet operation are presented in figures 20 and 21 for Mach numbers 2.93 and 1.88, respectively. The static-pressure coefficients were somewhat smaller at Mach 2.93 than at 1.88. These pressure distributions, which appeared to correspond to subsonic flow along the wedge, varied considerably and irregularly, although the trend of larger pressure coefficients with increasing values of  $h/\delta$  was observed for the two Mach numbers considered.

A pressure drag coefficient

$$C_{d_p} = \frac{1}{z_{\max}} \int_0^{z_{\max}} C_p dz$$

defined by these data was determined; the distributions are presented in figures 22 and 23 for Mach numbers 2.93 and 1.88, respectively. The pressure drag coefficient is plotted as a function of inlet mass flow for several values of  $h/\delta$ . The solid portions of the curve correspond to stable inlet operation. The pressure drag coefficient was found to increase steadily as the height of boundary-layer removal was increased.

Boundary-layer removal using cowl-lip scoop. - Cowl slots provide a method of allowing low-energy air which tends to accumulate in the corners of the inlet to escape by means of the pressure differential which exists across the lip. The effectiveness of this removal system is indicated in figure 14. It was proposed that a more positive method of keeping the boundary layer out of the inlet might be more effective and thus improve the inlet performance at the lower values of  $h/\delta$ . Accordingly, the cowl slot was modified into a cowl-lip scoop, the details of which were given in figures 1(d) and 1(e). This configuration was investigated in some detail at Mach 2.93 and less completely at Mach 1.88. The resulting pressure recovery - mass-flow characteristics of the inlet are presented in figures 24 and 25 for several values of  $h/\delta$ , where  $h$  is defined as the height of the slot. In these figures the reference pressure  $P_{1,D}$ , which by definition is the average total pressure ahead of the inlet in the projected area of the inlet, is arbitrarily held constant at the value corresponding to  $h/\delta$  of zero in figure 3 because of the difficulty in estimating the effective projected area of the inlet with this type of boundary-layer removal. (The cowl slot data in figure 14 have been corrected to this basis in transcribing the data from ref. 1.) Thus, in figure 24 for Mach 2.93, it may be observed that as the height of the cowl-lip scoop is increased, pressure

recovery increases; whereas the inlet mass flow generally decreases. At the largest scoop height tested ( $h/\delta$  of 1.254), the peak pressure recovery in terms of the average pressure ahead of the inlet was 54.9 percent. A peculiar double peak curve was noted for this value of  $h/\delta$ , with inlet instability occurring at the first peak. In figure 25 for Mach 1.88, the cowl-lip scoop was investigated only at  $h/\delta$  of 1.0 and 1.361. Considerably more mass flow was spilled at Mach 1.88 than at Mach 2.93.

Schlieren photographs of the inlet at peak pressure recovery are shown in figures 26 and 27. In figure 26 for Mach 2.93 a bow wave was observed at  $h/\delta$  of 1.254; the interaction of this wave with the conical shock and lambda form of the bow wave resulted in a twin vortex sheet near the lip which perhaps contributed to the unusual form of the pressure recovery variation with inlet mass flow. At the remaining values of  $h/\delta$ , the peak pressure condition was steady and no bow waves were noted. At Mach 1.88 figure 27 shows that a bow shock was also observed at  $h/\delta$  of 1.361 in accordance with the reduced inlet mass-flow ratio at the peak pressure condition.

Unstable inlet operation shock patterns for the two Mach numbers were identical. In figure 28(b) for the larger values of  $h/\delta$ , the shocks were confined to the spike. At the lower values of  $h/\delta$  the shock oscillation was extended to the plate, as shown in figure 28(a).

#### Comparison of Boundary-Layer-Removal Systems

As mentioned previously, the significance of  $h/\delta$  in the case of the cowl-lip scoop is not the same as with a scoop removal system. For the latter,  $h/\delta$  is a measure of that portion of the boundary layer prevented from entering the inlet. For the scoop removal configurations,  $P_{1,D}$  tends toward the free-stream total pressure as  $h/\delta$  is increased. In the case of the cowl-lip scoop,  $P_{1,D}$  was considered constant at the value corresponding to  $h/\delta$  equal to zero for the scoop removal systems. It is thus difficult to compare the inlet performance for the three systems of boundary-layer removal investigated herein on the basis of the average pressure ahead of the inlet. However, in the interests of consistency, figures 29(a) and 30(a) compare the inlet pressure recovery with the swept-scoop and deflection-wedge removal systems on the basis of  $P_{1,D}$ . For a comparison of all three systems, the pressure recovery is referenced to the free-stream total pressure  $P_0$  in figures 29(b) and 30(b). Figure 3 was used in the conversion.

In figure 29(b), for Mach 2.93, it may be observed that each system of boundary-layer removal gave approximately 48 percent total pressure recovery for  $h/\delta$  greater than 1.2. The peak values of



total-pressure recovery varied only slightly from 49 percent and occurred at appreciably different values of scoop height parameter. The total-pressure recovery obtained using the ram scoop was 51.5 percent, as mentioned previously.

Similarly, peak total-pressure recovery data for the three systems of boundary-layer removal at Mach 1.88 are presented in figure 30(b). It was noted that each system of boundary-layer removal investigated herein and the ram scoop gave comparable total-pressure recoveries of 89 percent, although a larger scoop height was required for the wedge and cowl-lip scoop systems. A comparison of the cowl slot of figure 14 with the cowl-lip scoop of the present investigation indicates that at large values of  $h/\delta$  the pressure recovery of the cowl-lip scoop is slightly higher than that obtained with the original cowl slot. At low values of  $h/\delta$  direct comparisons cannot be made because of the lack of data in the present investigation, although the general fairing of the curves indicates that the cowl slot and cowl-lip scoop are comparable.

Although cowl-lip scoop and wedge removal systems would not generally be expected to yield the same variation of inlet pressure recovery with  $h/\delta$  as would the conventional boundary-layer scoop, some explanation is believed required for the discrepancy between the inlet performance with scoops and with wedges. It should be noted that the wedge studied in the present investigation had a half-angle greater than the compression cone half-angle; hence the wedge shock (even if attached) would lie ahead of the leading edge of the splitter plate which was swept nearly at the conical shock angle. Detachment of the wedge shock due to the boundary layer would aggravate this condition. For example, at  $h/\delta$  of 1.0, some of the boundary layer behind the shock from the wedge would flow up and over the splitter plate into the inlet. Thus it might be expected that an  $h/\delta$  greater than 1.0 would be required to keep the low-energy air out of the inlet. It might also be expected that a reduction in sweep of the splitter plate would reduce the upflow of low-energy air into the inlet.

For a somewhat similar wedge-inlet combination in reference 9 there were indications of better wedge effectiveness. The wedge in that example was beveled at  $30^\circ$ . Also, unpublished data from the authors of references 3 and 4, for two-dimensional compression ramp and spike-type inlets, respectively, have shown equivalent inlet pressure recovery - mass-flow characteristics with wedge and scoop removal systems at  $h/\delta$  of 1.0. The wedge included angle was approximately the same as the angle of the present tests. One appreciable difference in the configurations was that in references 3 and 4 the leading edge of the wedge was set aft of the leading edge of the splitter plate by approximately 20 percent of the distance to the lip of the inlet. The oil-flow

technique mentioned previously showed that as the wedge was moved aft beneath the splitter plate, the detached bow shock in front of the wedge tended to follow. The rather effective boundary-layer removal observed in even the extreme case of reference 1, when complete blockage of the flow beneath the swept splitter plate was allowed considerably downstream of the inlet lip, is thus reasonable if the bow shock is also downstream of the inlet lip.

In summary, then, the deflection wedge system of removal should be more effective if one or more of the following steps are taken: (1) the wedge is located downstream of the apex of the cone, (2) the wedge included angle is reduced, and (3) the sweep of the splitter plate is reduced.

An additional indication of the effectiveness of the three systems of boundary-layer removal is given in figures 31 and 32 for Mach numbers of 2.93 and 1.88, respectively. The mass-flow ratio  $m_D/m_{(D+s),0}$  for critical inlet operation is plotted as a function of  $h/\delta$ . The mass flow  $m_{(D+s),0}$  represents the theoretical mass flow passing through the stream tube of the projected inlet plus boundary-layer-removal system at free-stream conditions and is directly proportional to the total projected area. The mass-flow ratio  $m_D/m_{(D+s),0}$  is therefore indicative of the inlet mass flow per unit total projected area. An indication of the relative sizes of the inlet installations required to deliver the same amount of inlet mass flow at equivalent pressure recoveries may be obtained from these figures. At the  $h/\delta$  at which maximum pressure recovery was attained (indicated by flagged symbols in figs. 31 and 32), it may be seen that at Mach 2.93 the inlet mass flow per unit total projected area is largest for the cowl-lip removal system; or, to capture the same amount of inlet mass flow, the required total projected area of the cowl-lip scoop inlet is smaller than for the scoop- and wedge-type inlets. At the lower Mach number (fig. 32), the required projected areas are essentially equivalent for the cowl-lip scoop and inlet-scoop configurations, while the wedge removal configuration requires slightly larger inlet. Improvement in the design of the wedge installation would probably result in only small differences in total projected area of the three installations.

#### SUMMARY OF RESULTS AND CONCLUSIONS

An experimental investigation to compare several systems of boundary-layer removal ahead of a typical conical external-compression side inlet yielded the following results:

1. The maximum total-pressure recoveries observed at Mach numbers of 1.88 and 2.93 were approximately 89 and 49 percent, respectively, for all systems of boundary-layer removal investigated. This compares with 89 and 51.5 percent previously obtained with the same inlet utilizing the ram-scoop removal system.

2. The swept-leading-edge boundary-layer scoop was found to offer only slight improvements in the reduction of inlet sensitivity to the boundary-layer-scoop mass-flow ratio over that previously observed with a ram-type boundary-layer scoop. The effect of scoop instability on the inlet was reduced slightly by use of the swept scoop.

3. Two alternative systems of boundary-layer removal, namely, the deflection wedge and the cowl-lip scoop, were found to provide inlet total-pressure recoveries comparable with those of the scoop removal systems provided slightly increased values of boundary-layer scoop height were utilized.

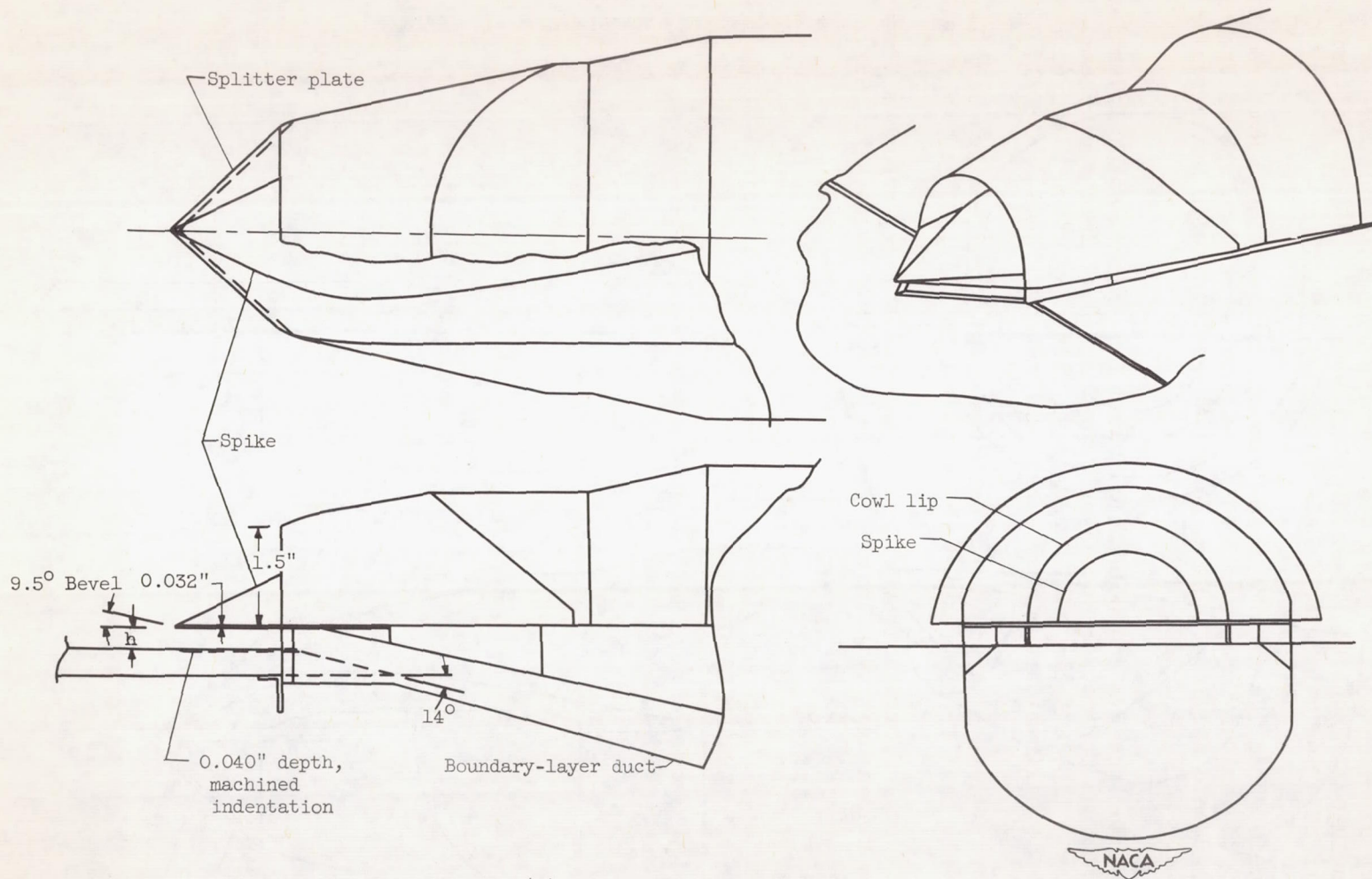
4. At equivalent pressure recoveries the cowl-lip scoop spilled the least amount of air and indicated a total projected frontal area of inlet plus scoop as small as or smaller than the inlet with conventional scoop or wedge removal systems.

Lewis Flight Propulsion Laboratory  
National Advisory Committee for Aeronautics  
Cleveland, Ohio, June 5, 1953

#### REFERENCES

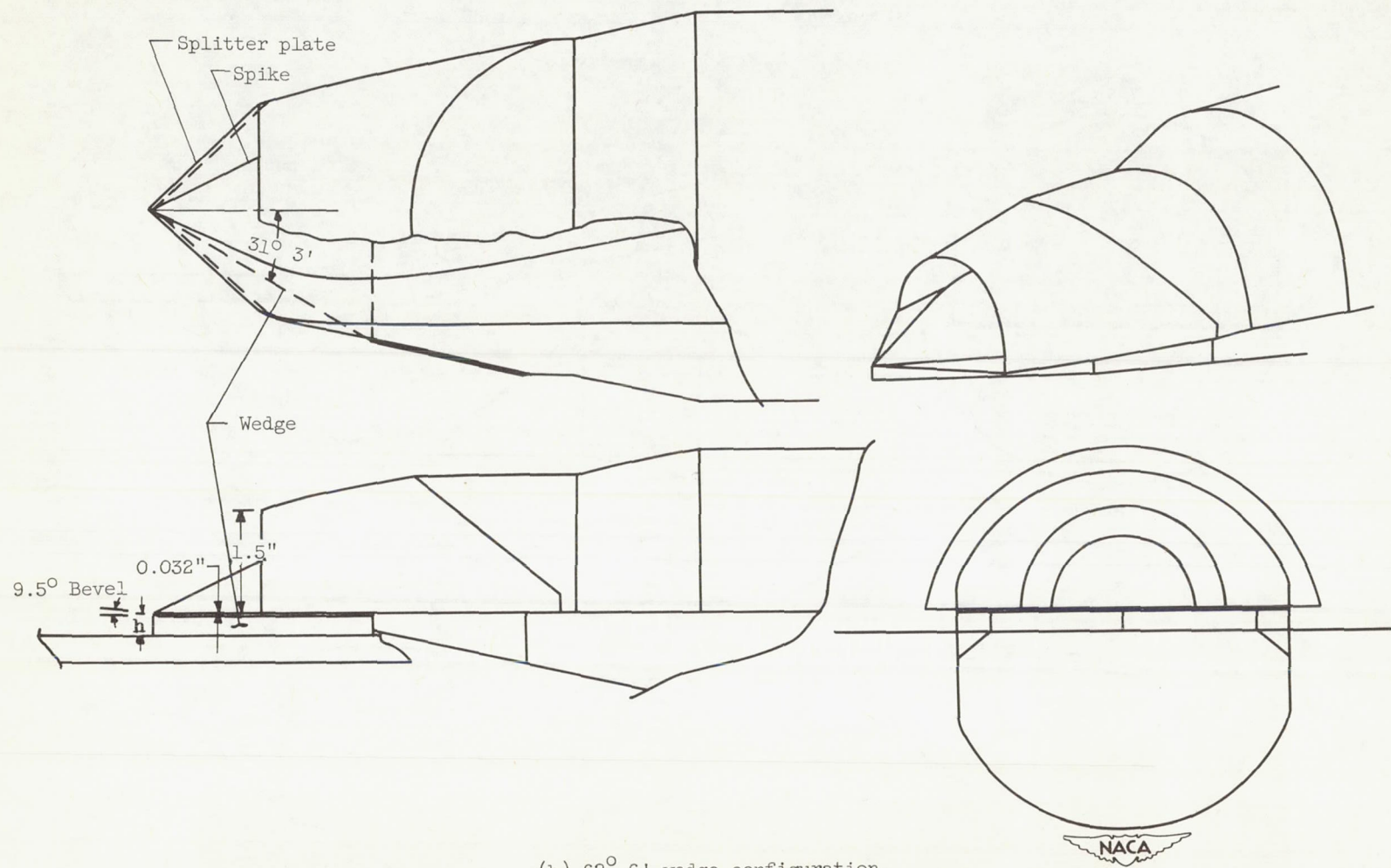
1. Goelzer, H. Fred, and Cortright, Edgar M., Jr.: Investigation at Mach Number 1.88 of Half of a Conical-Spike Diffuser Mounted as a Side Inlet with Boundary-Layer Control. NACA RM E51G06, 1951.
2. Piercy, Thomas G., and Johnson, Harry W.: Investigation at Mach Number 2.93 of Half of a Conical-Spike Diffuser Mounted as a Side Inlet with Boundary-Layer Control. NACA RM E52G23, 1952.
3. Valerino, Alfred S.: Performance Characteristics at Mach Numbers to 2.0 of Various Types of Side Inlets Mounted on Fuselage of Proposed Supersonic Airplane. I - Two-Dimensional Compression-Ramp Inlets with Semicircular Cowls. NACA RM E52E02, 1952.

4. Allen, J. L., and Simon, P. C.: Performance Characteristics at Mach Numbers to 2.0 of Various Types of Side Inlets Mounted on Fuselage of Proposed Supersonic Airplane. II - Inlets Utilizing Half of a Conical Spike. NACA RM E52G08, 1952.
5. Esenwein, Fred T.: Performance Characteristics at Mach Numbers to 2.0 of Various Types of Side Inlets Mounted on Fuselage of Proposed Supersonic Airplane. III - Normal-Wedge Inlet with Semicircular Cowl. NACA RM E52H20, 1952.
6. Davis, Wallace F., and Goldstein, David L.: Experimental Investigation at Supersonic Speeds of Twin-Scoop Duct Inlets of Equal Area. II - Effects of Slots upon an Inlet Enclosing 61.5 Percent of the Maximum Circumference of the Forebody. NACA RM A8C11, 1948.
7. Tucker, Maurice: Approximate Calculation of Turbulent Boundary-Layer Development in Compressible Flow. NACA TN 2337, 1951.
8. McLafferty, George: Theoretical Pressure Recovery Through a Normal Shock in a Duct with Initial Boundary Layer. Jour. Aero. Sci., vol. 20, no. 3, Mar. 1953, pp. 169-174.
9. Wittliff, Charles E., and Byrne, Robert W.: Preliminary Investigation of a Supersonic Scoop Inlet Derived from a Conical-Spike Nose Inlet. NACA RM L51G11, 1951.



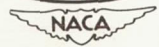
(a) Swept-scoop configuration

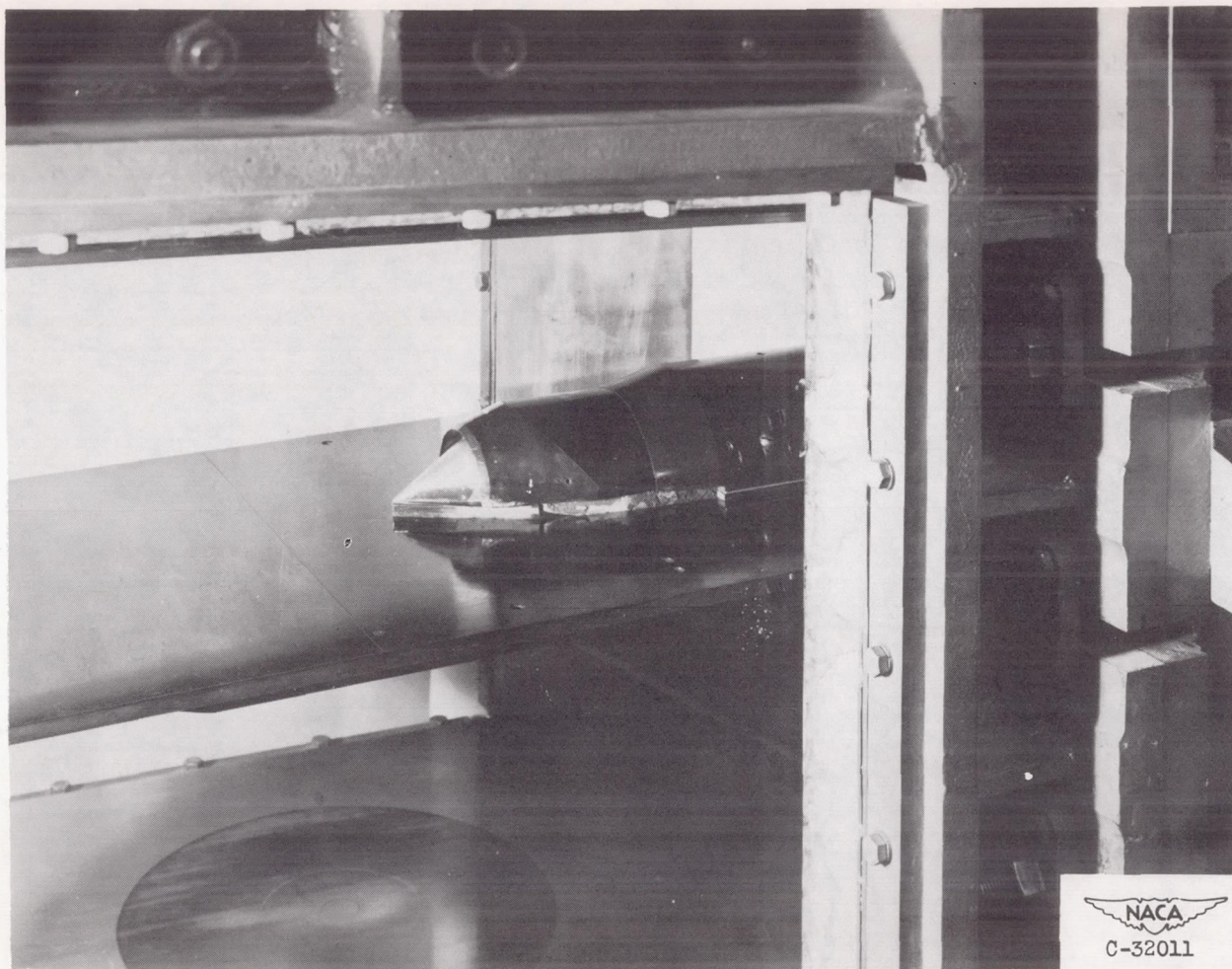
Figure 1. - Boundary-layer-removal systems.



(b) 62° 6' wedge configuration.

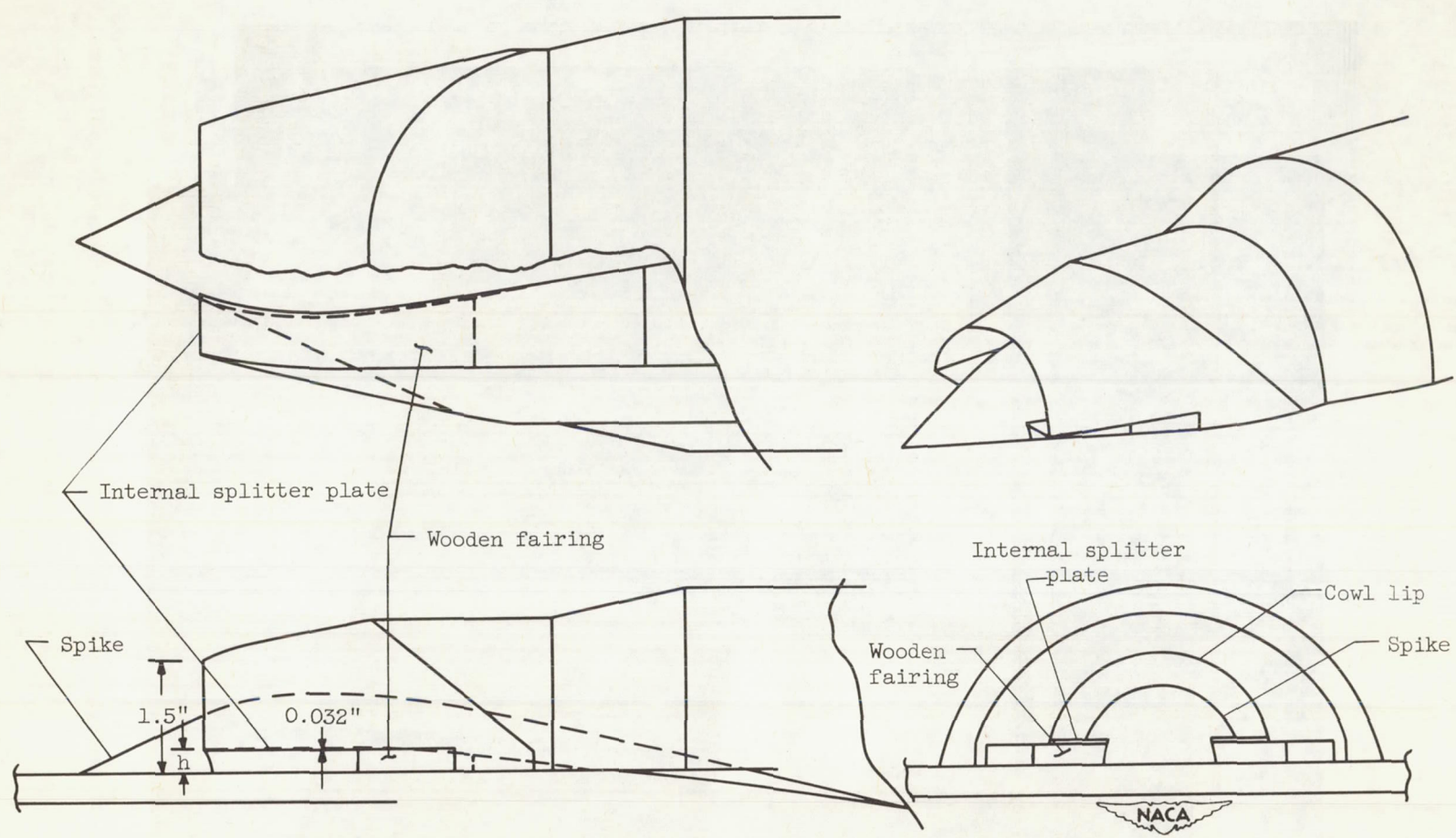
Figure 1. - Continued. Boundary-layer-removal systems.





(c) Photograph of wedge model installed in 18- by 18-inch Mach 3.05 tunnel.

Figure 1. - Continued. Boundary-layer-removal systems.

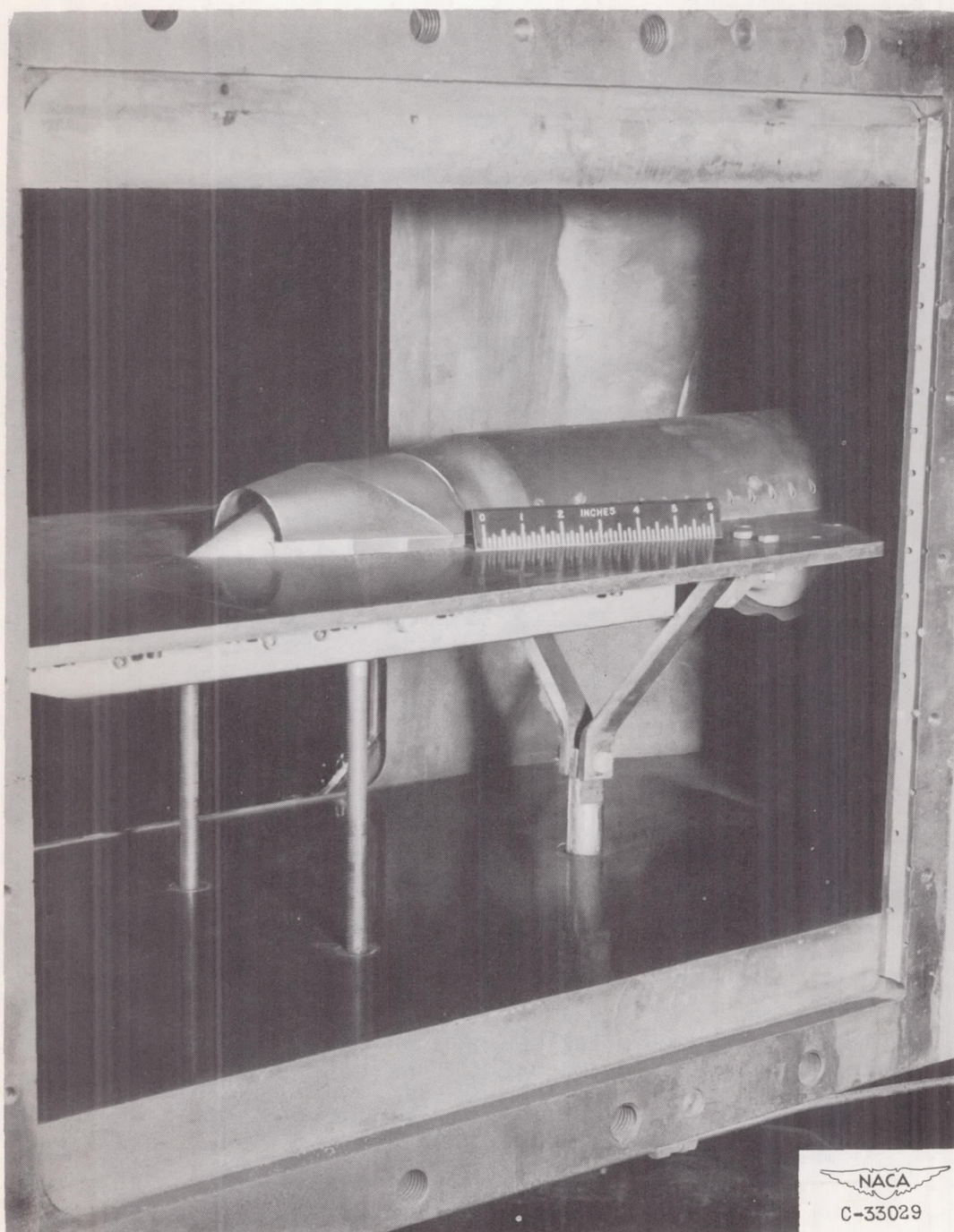


(d) Cowl-lip scoop.

Figure 1. - Continued. Boundary-layer-removal systems.



2944



(e) Photograph of cowl-lip scoop model installed in 18- by 18-inch Mach 1.91 tunnel.  
Figure 1. - Concluded. Boundary-layer-removal systems.

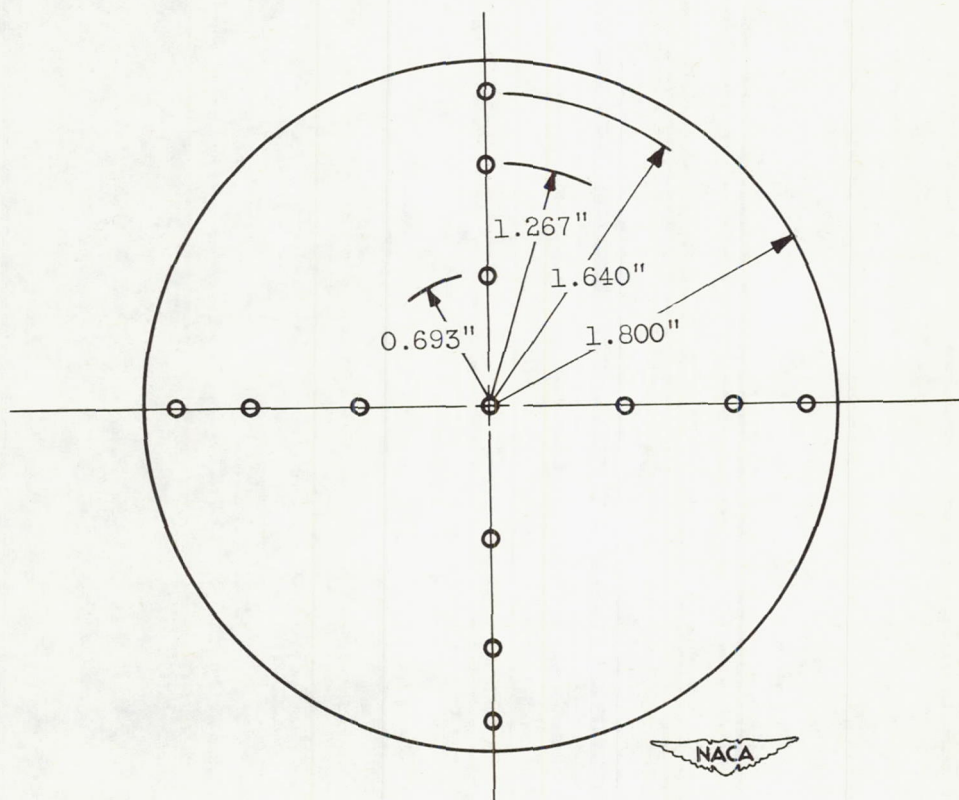


Figure 2. - Location of pitot-static tubes in diffuser pressure rake. 18- by 18-inch Mach 1.91 tunnel.

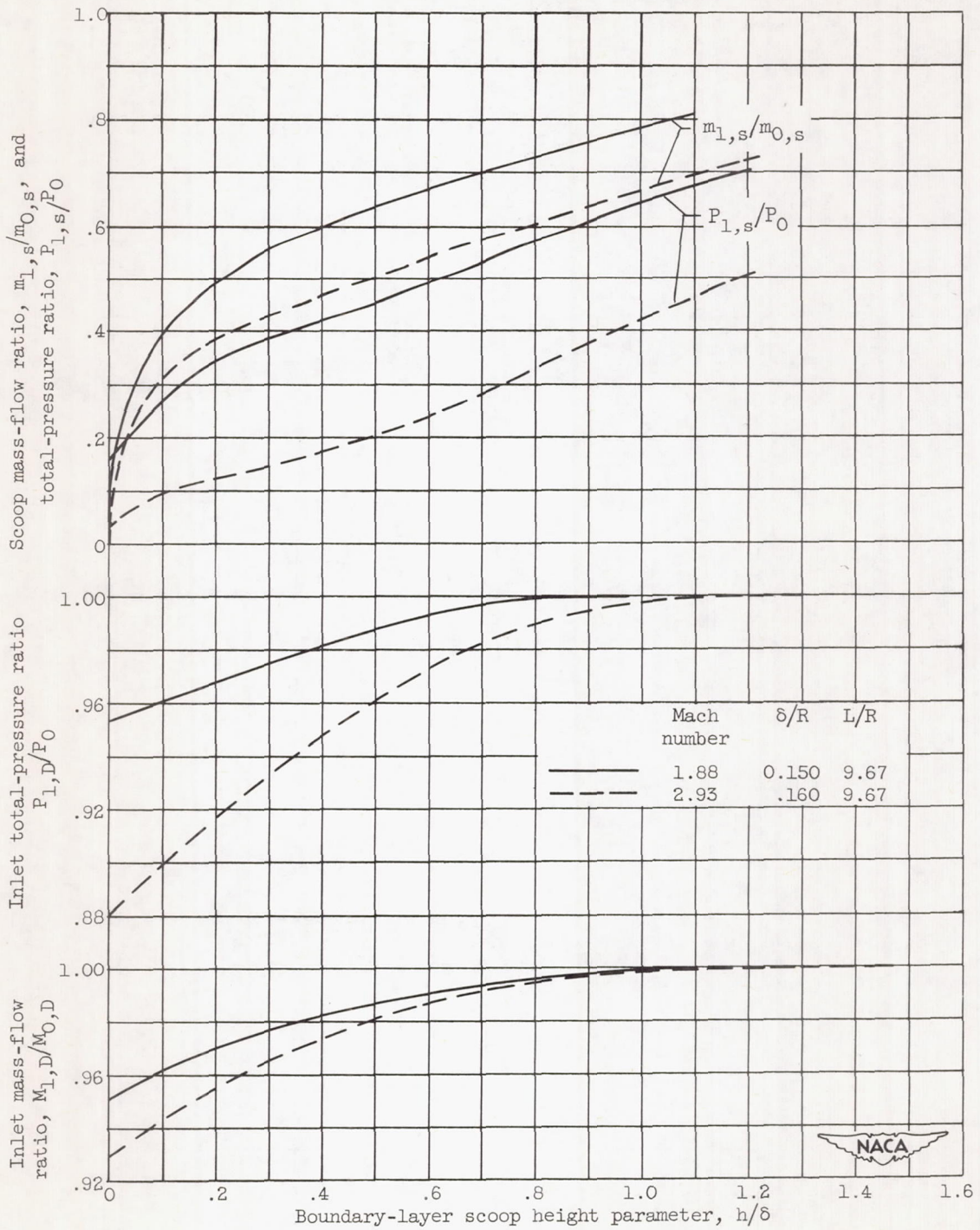


Figure 3. - Summary of effect of presence of boundary layer on mass flow and total pressure ahead of inlet and boundary-layer scoop.

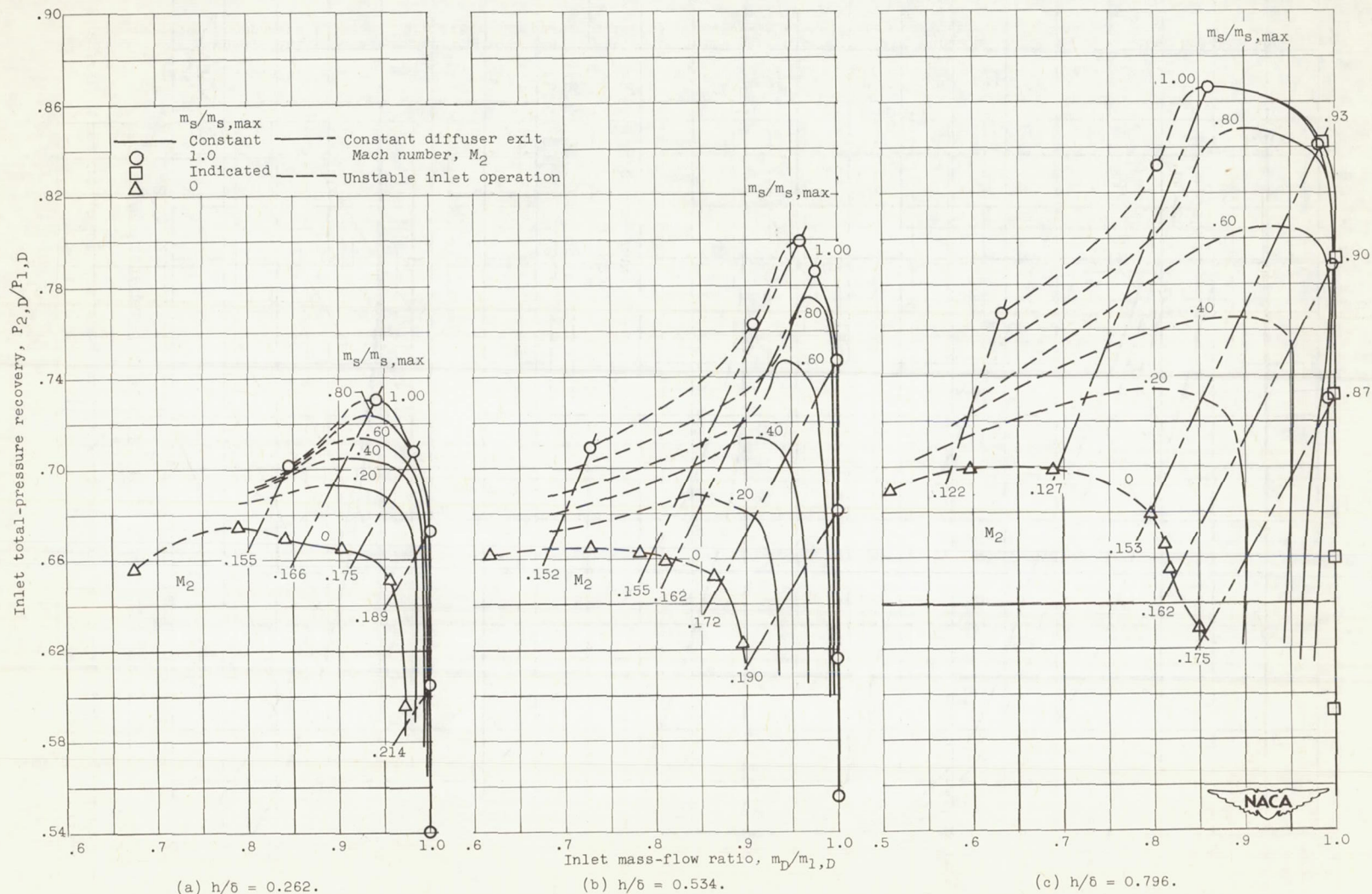


Figure 4. - Inlet total-pressure recovery as function of inlet mass-flow ratio for various boundary-layer scoop heights and boundary-layer scoop mass flows at Mach 1.88. Swept-scoop inlet; boundary-layer thickness parameter, 0.150.

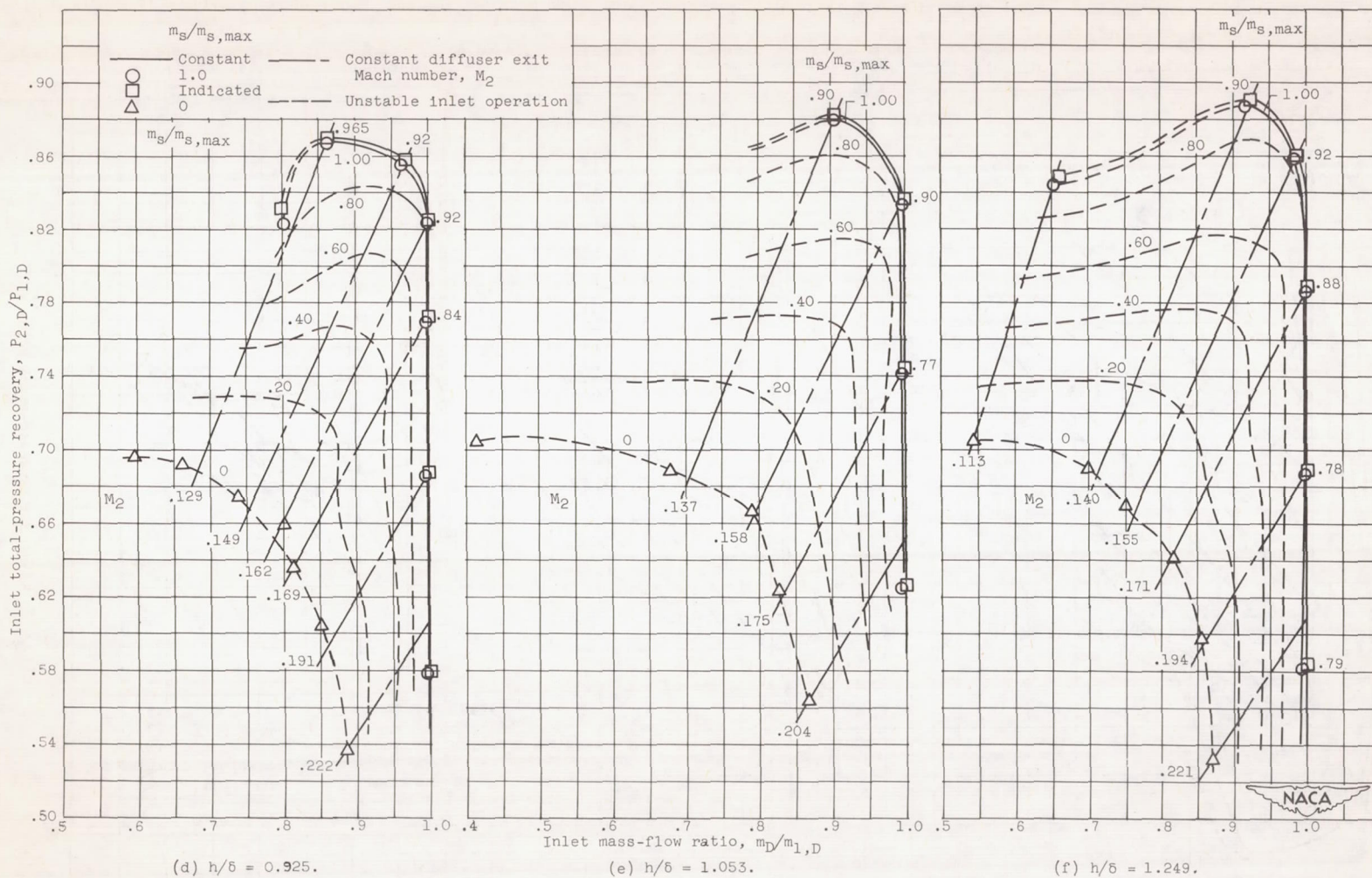


Figure 4. - Concluded. Inlet total-pressure recovery as function of inlet mass-flow ratio for various boundary-layer scoop heights and boundary-layer scoop mass flows at Mach 1.88. Swept-scoop inlet; boundary-layer thickness parameter, 0.150.

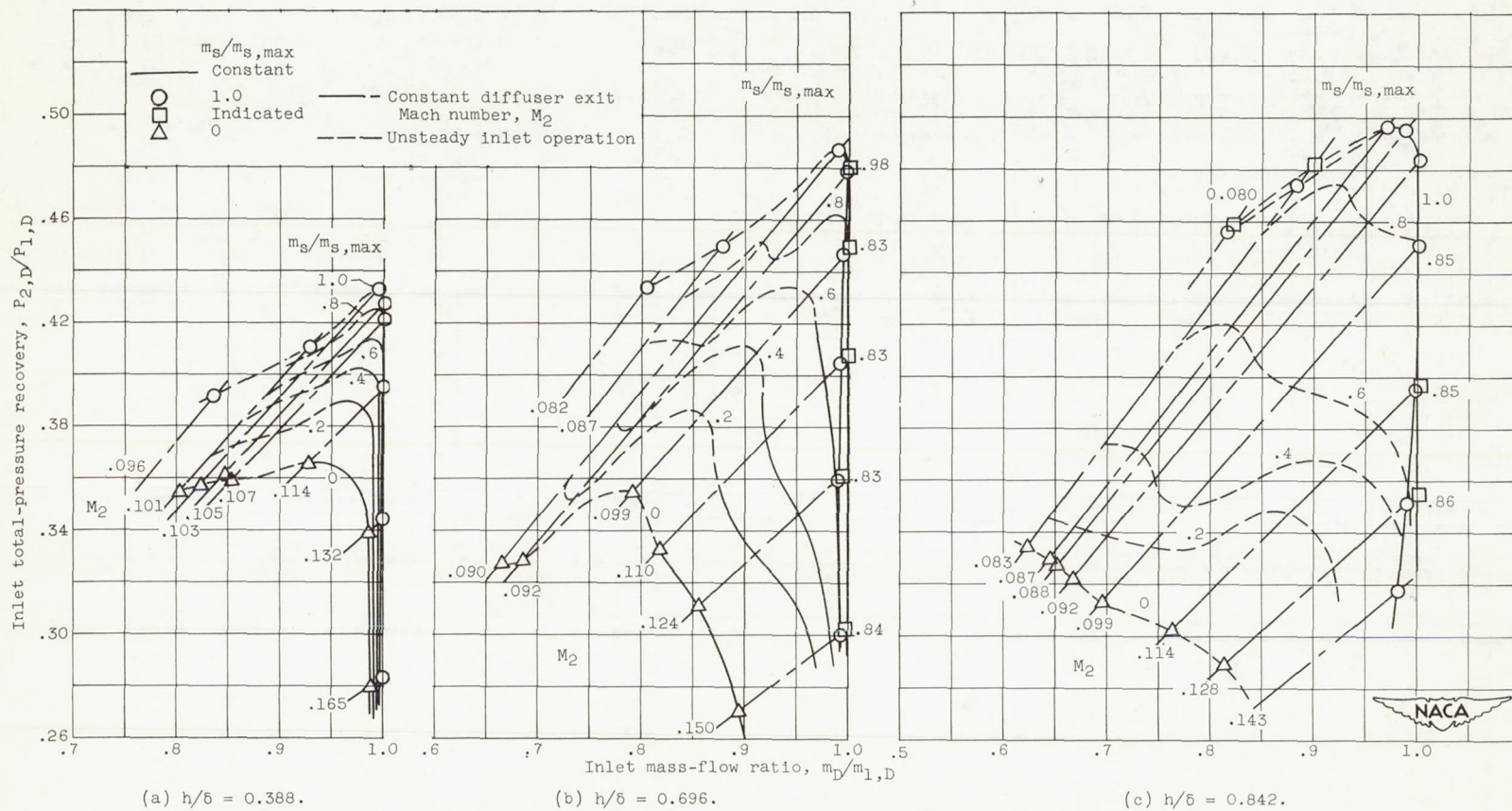


Figure 5. - Inlet total-pressure recovery as function of inlet mass-flow ratio for various boundary-layer scoop heights and boundary-layer scoop mass flows at Mach 2.93. Swept-scoop inlet; boundary-layer thickness parameter, 0.160.

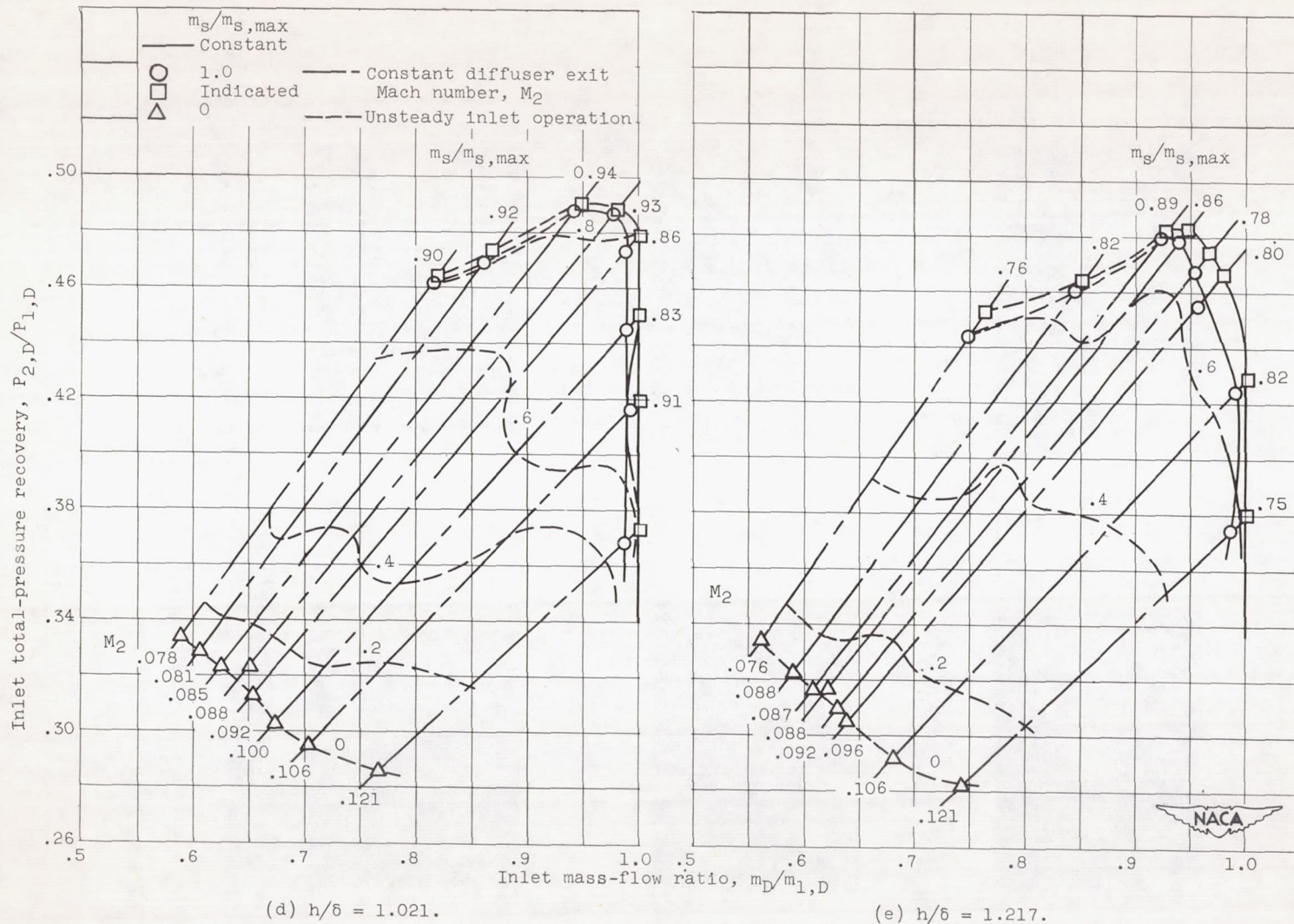
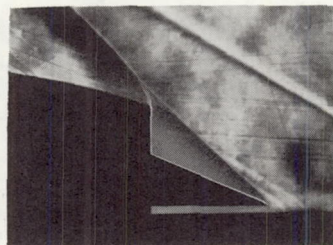
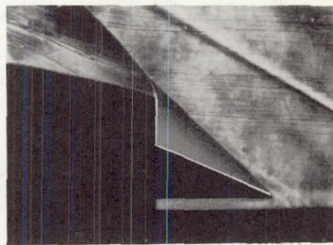


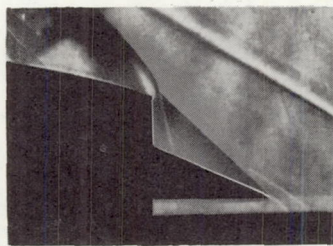
Figure 5. - Concluded. Inlet total-pressure recovery as function of inlet mass-flow ratio for various boundary-layer scoop heights and boundary-layer scoop mass flows at Mach 2.93. Swept-scoop inlet; boundary-layer thickness parameter, 0.160.



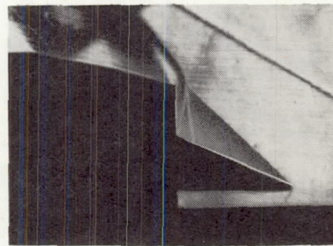
(a)  $h/\delta$ , 0.262;  $P_{2,D}/P_{1,D}$ , 0.730;  
 $m_D/m_{1,D}$ , 0.940;  $m_S/m_{S,max}$ , 1.00.



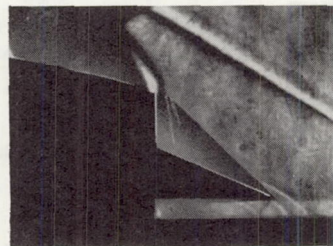
(b)  $h/\delta$ , 0.534;  $P_{2,D}/P_{1,D}$ , 0.800;  
 $m_D/m_{1,D}$ , 0.959;  $m_S/m_{S,max}$ , 1.00.



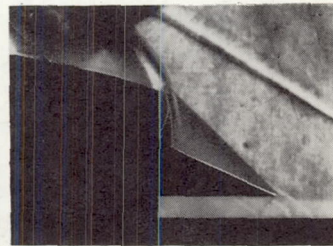
(c)  $h/\delta$ , 0.796;  $P_{2,D}/P_{1,D}$ , 0.866;  
 $m_D/m_{1,D}$ , 0.859;  $m_S/m_{S,max}$ , 1.00.



(d)  $h/\delta$ , 0.925;  $P_{2,D}/P_{1,D}$ , 0.869;  
 $m_D/m_{1,D}$ , 0.862;  $m_S/m_{S,max}$ , 0.965.



(e)  $h/\delta$ , 1.053;  $P_{2,D}/P_{1,D}$ , 0.883;  
 $m_D/m_{1,D}$ , 0.906;  $m_S/m_{S,max}$ , 0.902.



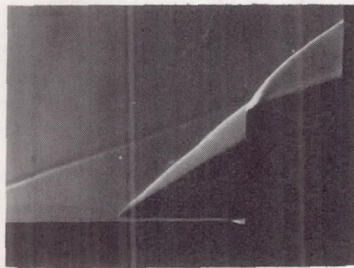
(f)  $h/\delta$ , 1.249;  $P_{2,D}/P_{1,D}$ , 0.891;  
 $m_D/m_{1,D}$ , 0.923;  $m_S/m_{S,max}$ , 0.905.

NACA  
 C-33030

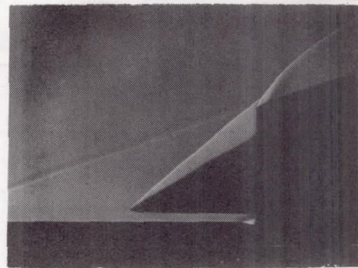
Figure 6. - Steady schlieren photographs of peak pressure conditions for swept-scoop model at Mach 1.88.



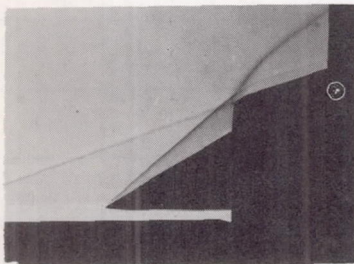
2944



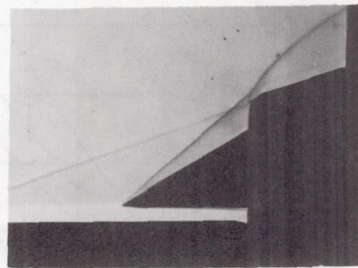
(a)  $h/\delta$ , 0.388;  $P_{2,D}/P_{1,D}$ , 0.432;  
 $m_D/m_{1,D}$ , 0.995;  $m_s/m_{s,max}$ , 0.958.



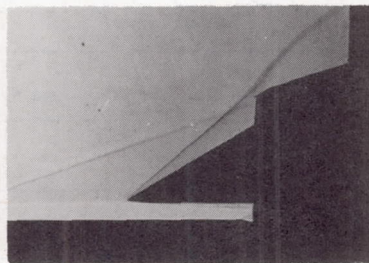
(b)  $h/\delta$ , 0.696;  $P_{2,D}/P_{1,D}$ , 0.486;  
 $m_D/m_{1,D}$ , 0.988;  $m_s/m_{s,max}$ , 1.00.



(c)  $h/\delta$ , 0.842;  $P_{2,D}/P_{1,D}$ , 0.496;  
 $m_D/m_{1,D}$ , 0.969;  $m_s/m_{s,max}$ , 1.00.



(d)  $h/\delta$ , 1.021;  $P_{2,D}/P_{1,D}$ , 0.491;  
 $m_D/m_{1,D}$ , 0.948;  $m_s/m_{s,max}$ , 0.942.



(e)  $h/\delta$ , 1.217;  $P_{2,D}/P_{1,D}$ , 0.483;  
 $m_D/m_{1,D}$ , 0.947;  $m_s/m_{s,max}$ , 0.883.

NACA  
 C-33031

Figure 7. - Steady schlieren photographs of peak pressure conditions for swept-scoop model at Mach 2.93.

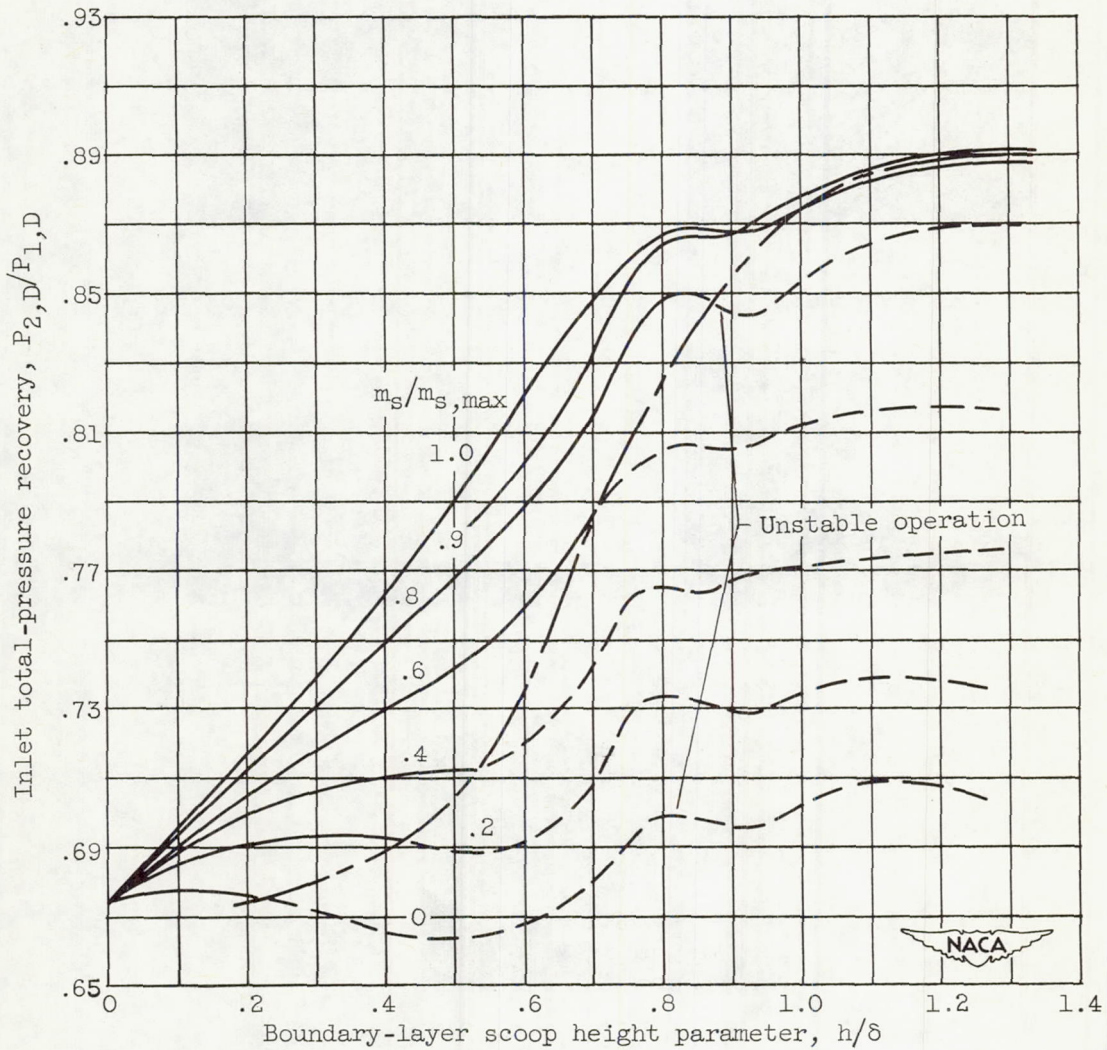


Figure 8. - Summary of effect of boundary-layer removal on peak total-pressure recovery of side inlet with swept scoop at Mach 1.88.

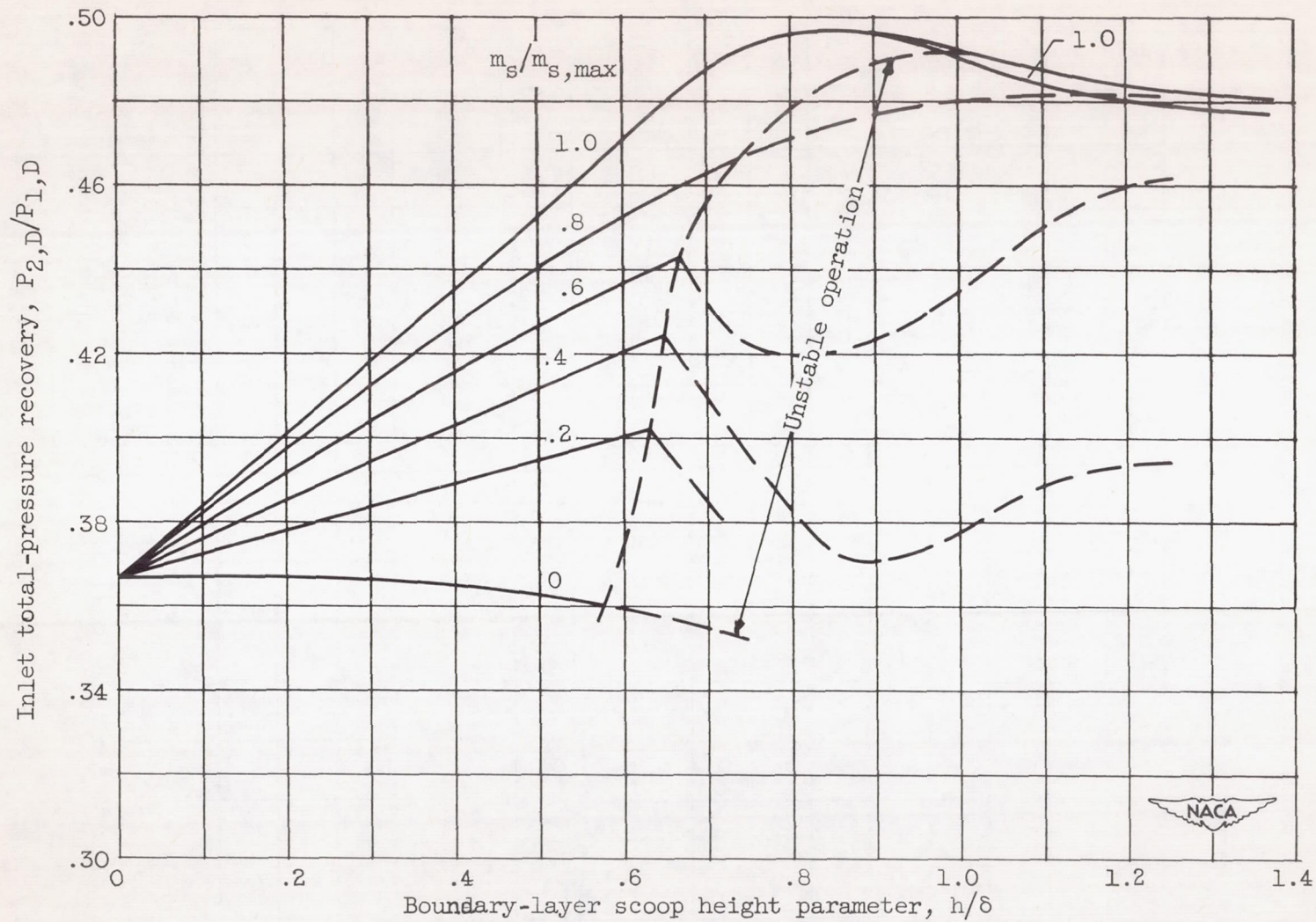


Figure 9. - Summary of effect of boundary-layer removal on peak total-pressure recovery of side inlet with swept scoop at Mach 2.93.

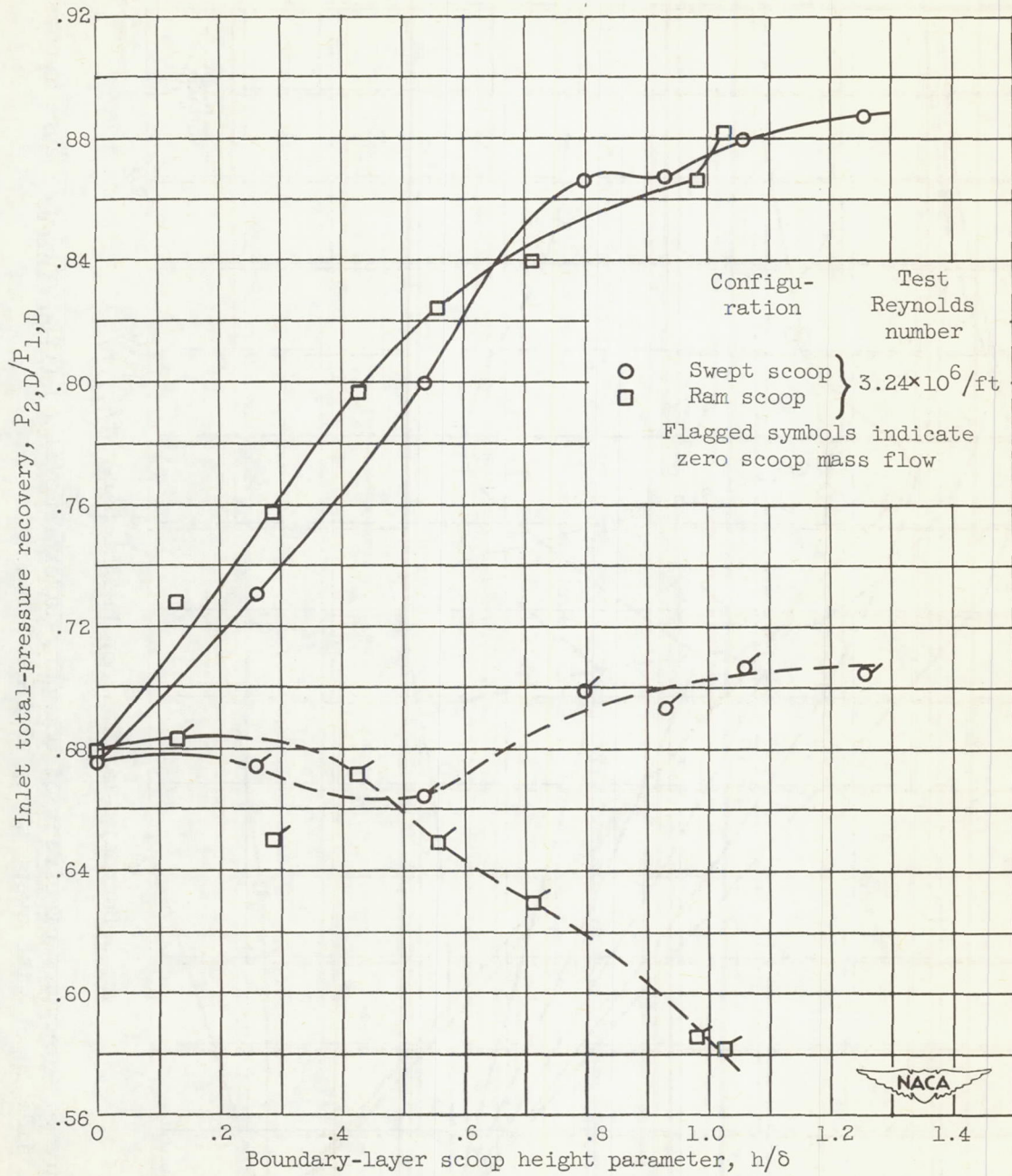
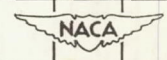


Figure 10. - Comparison of peak total-pressure recoveries of side inlets with ram and swept scoops at Mach 1.88.

2944



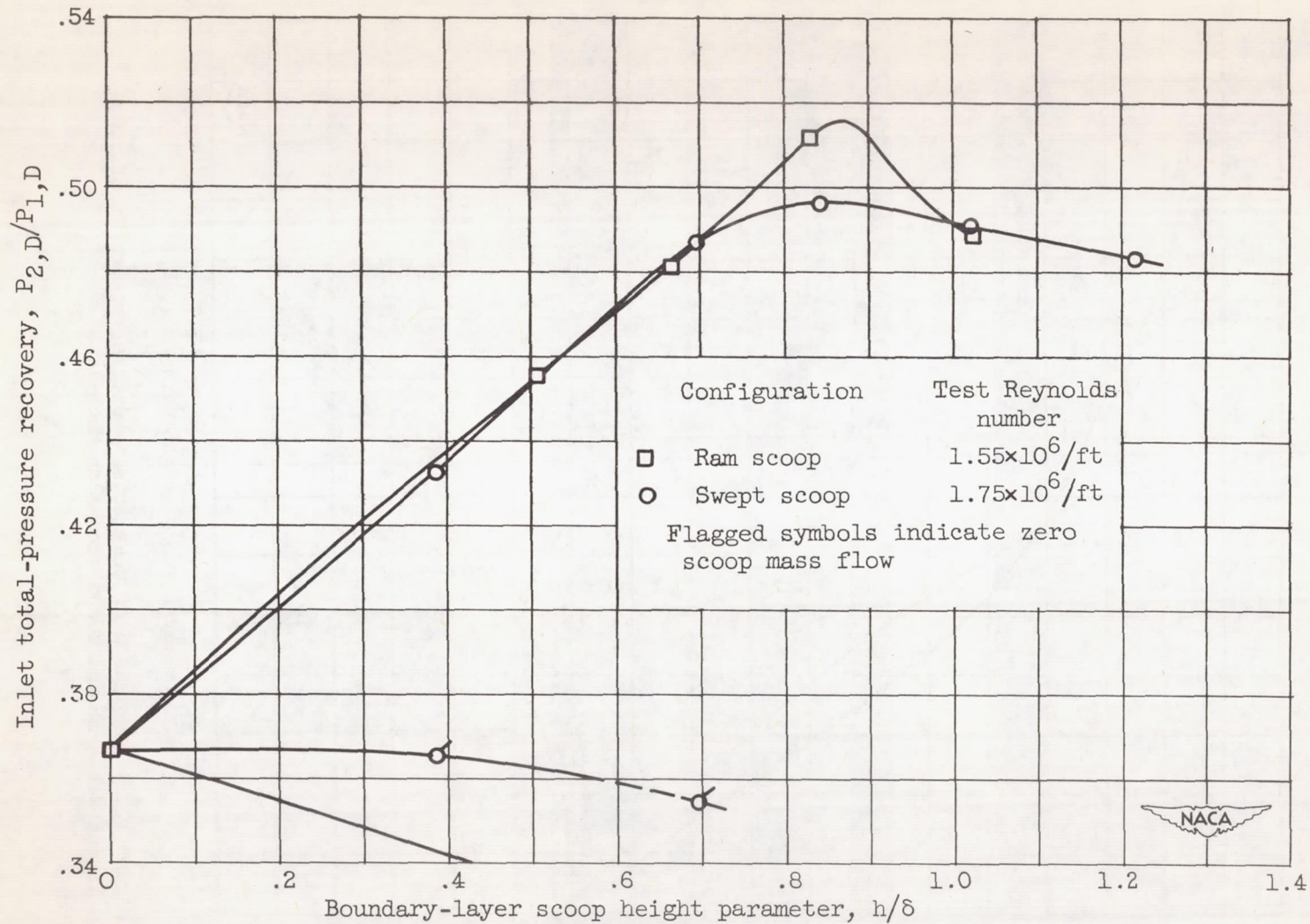
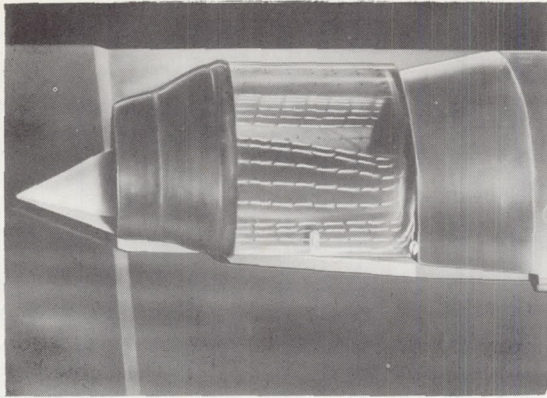
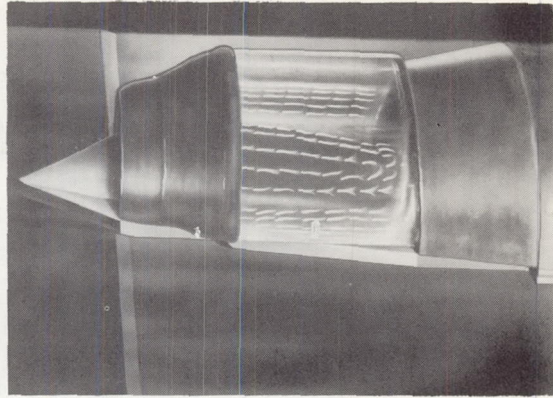


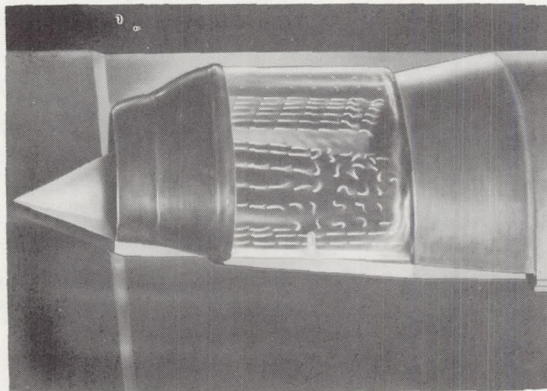
Figure 11. - Comparison of peak total-pressure recoveries of side inlets with ram and swept scoops at Mach 2.93.



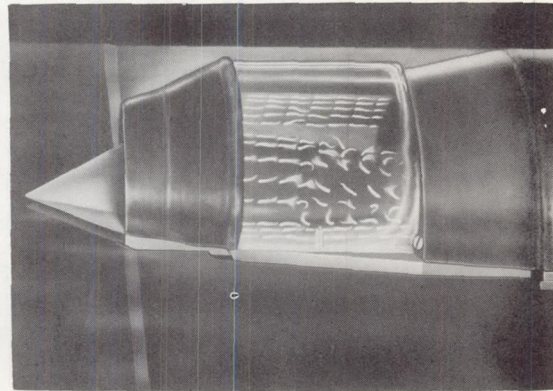
(a)  $h/\delta$ , 0.992;  $P_{2,D}/P_{1,D}$ , 0.491;  
 $m_D/m_{1,D}$ , 1.00.



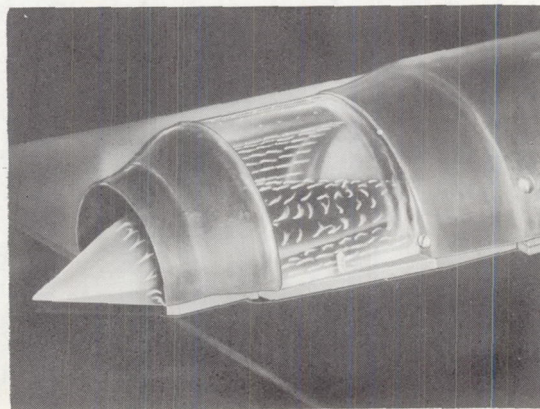
(b)  $h/\delta$ , 0.992;  $P_{2,D}/P_{1,D}$ , 0.519;  
 $m_D/m_{1,D}$ , 1.00.



(c)  $h/\delta$ , 0.992;  $P_{2,D}/P_{1,D}$ , 0.563;  
 $m_D/m_{1,D}$ , 1.00.



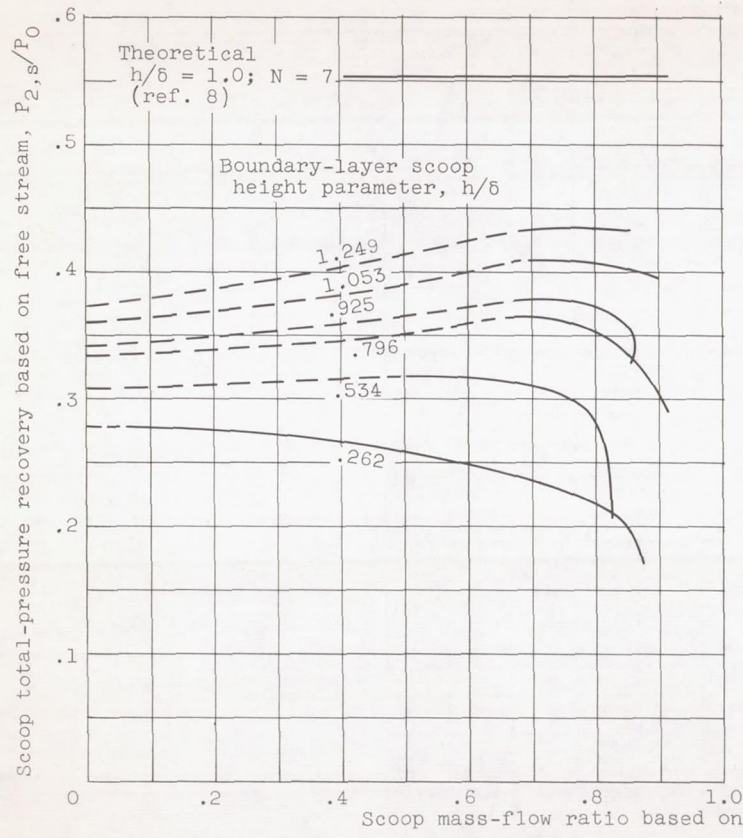
(d)  $h/\delta$ , 0.992;  $P_{2,D}/P_{1,D}$ , 0.618.  
 $m_D/m_{1,D}$ , 0.981.



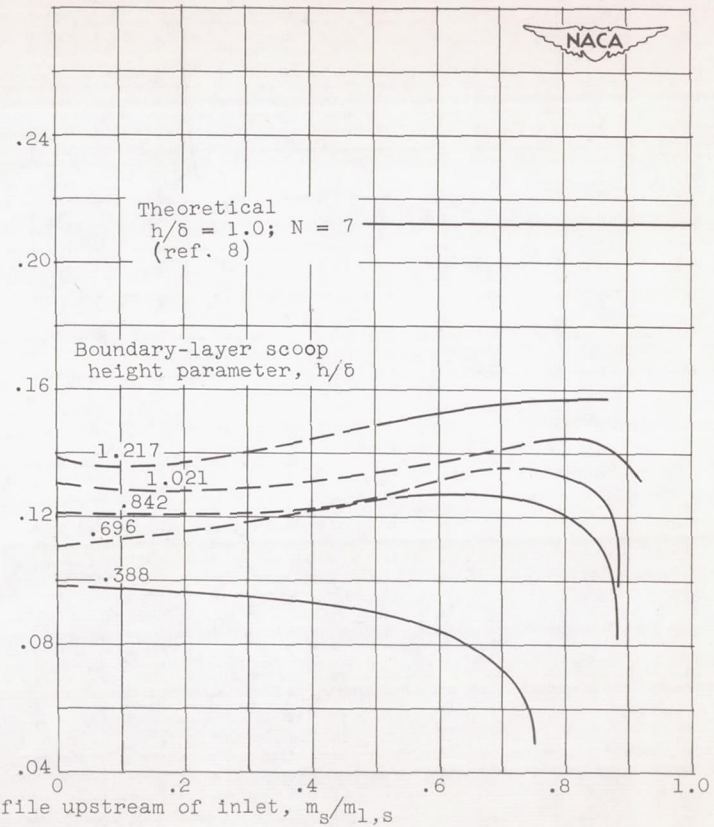
(e)  $h/\delta$ , 0.992;  $P_{2,D}/P_{1,D}$ , 0.869;  
 $m_D/m_{1,D}$ , 0.880.

NACA  
 C-33032

Figure 12. - Tuft study showing movement of internal shock.



(a) Mach 1.88.



(b) Mach 2.93.

Figure 13. - Comparison of scoop total-pressure recovery as function of scoop mass flow for swept-scoop configurations at Mach numbers 1.88 and 2.93.

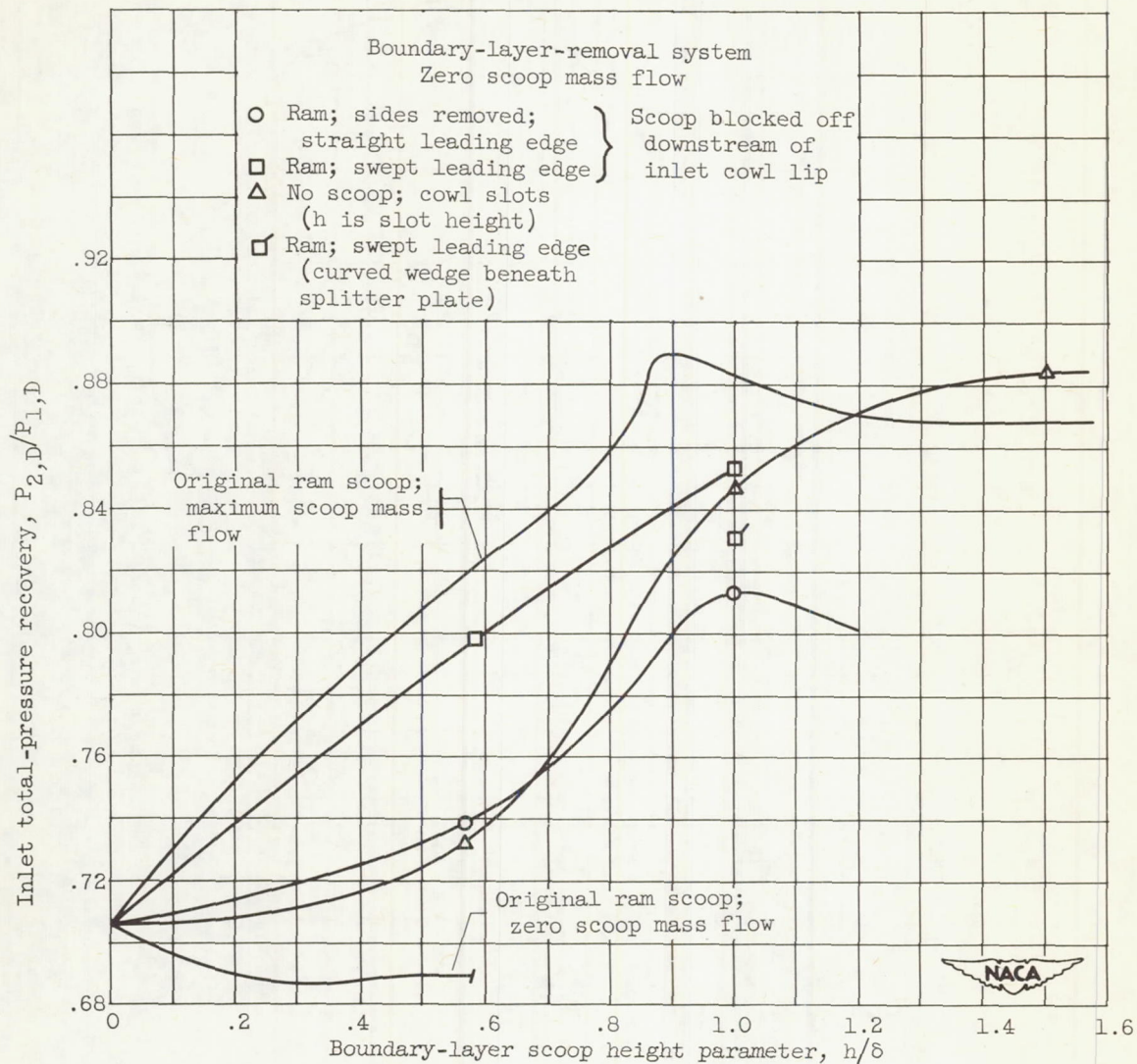


Figure 14. - Summary of peak total-pressure recovery for several systems of boundary-layer removal at Mach 1.88. Boundary-layer thickness parameter  $\delta/R$ , 0.093.



2944

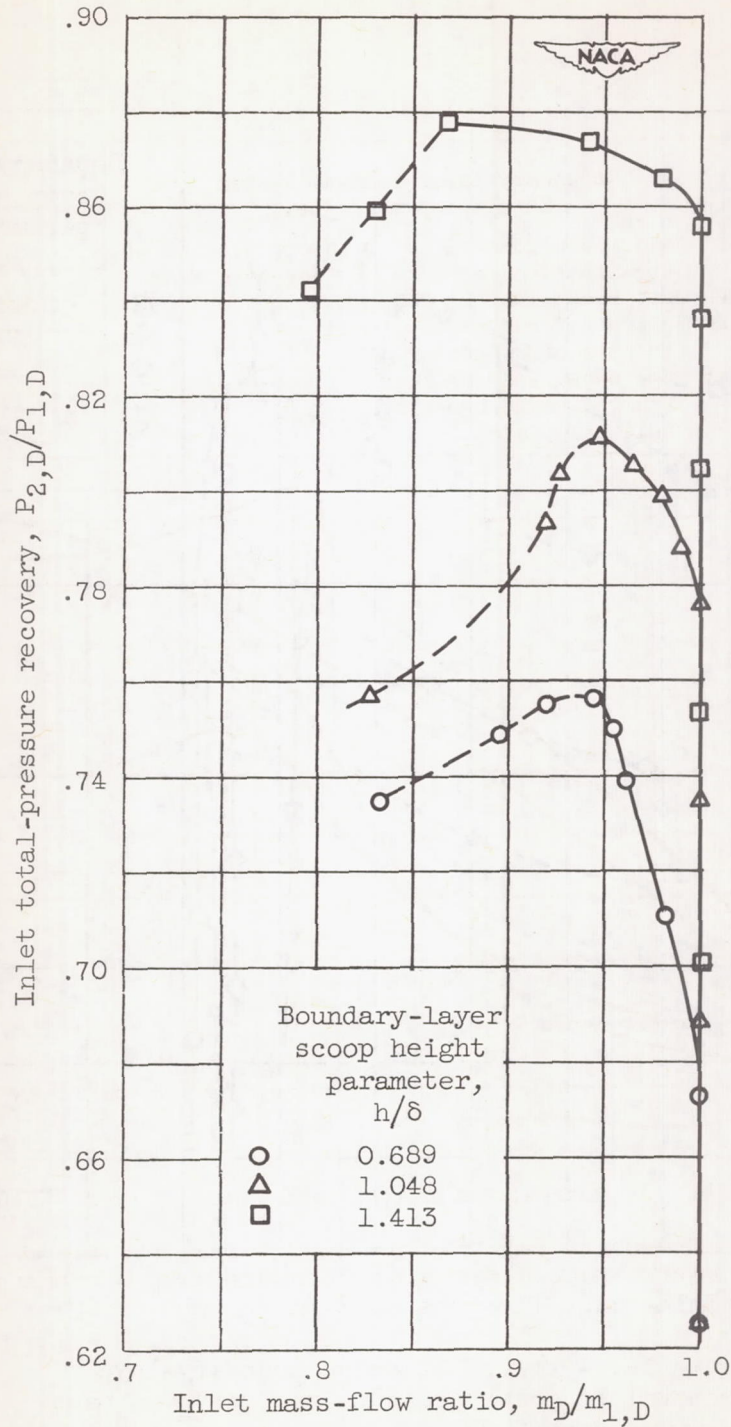


Figure 15. - Effect of wedge boundary-layer removal on inlet pressure recovery and mass flow at Mach 1.88.

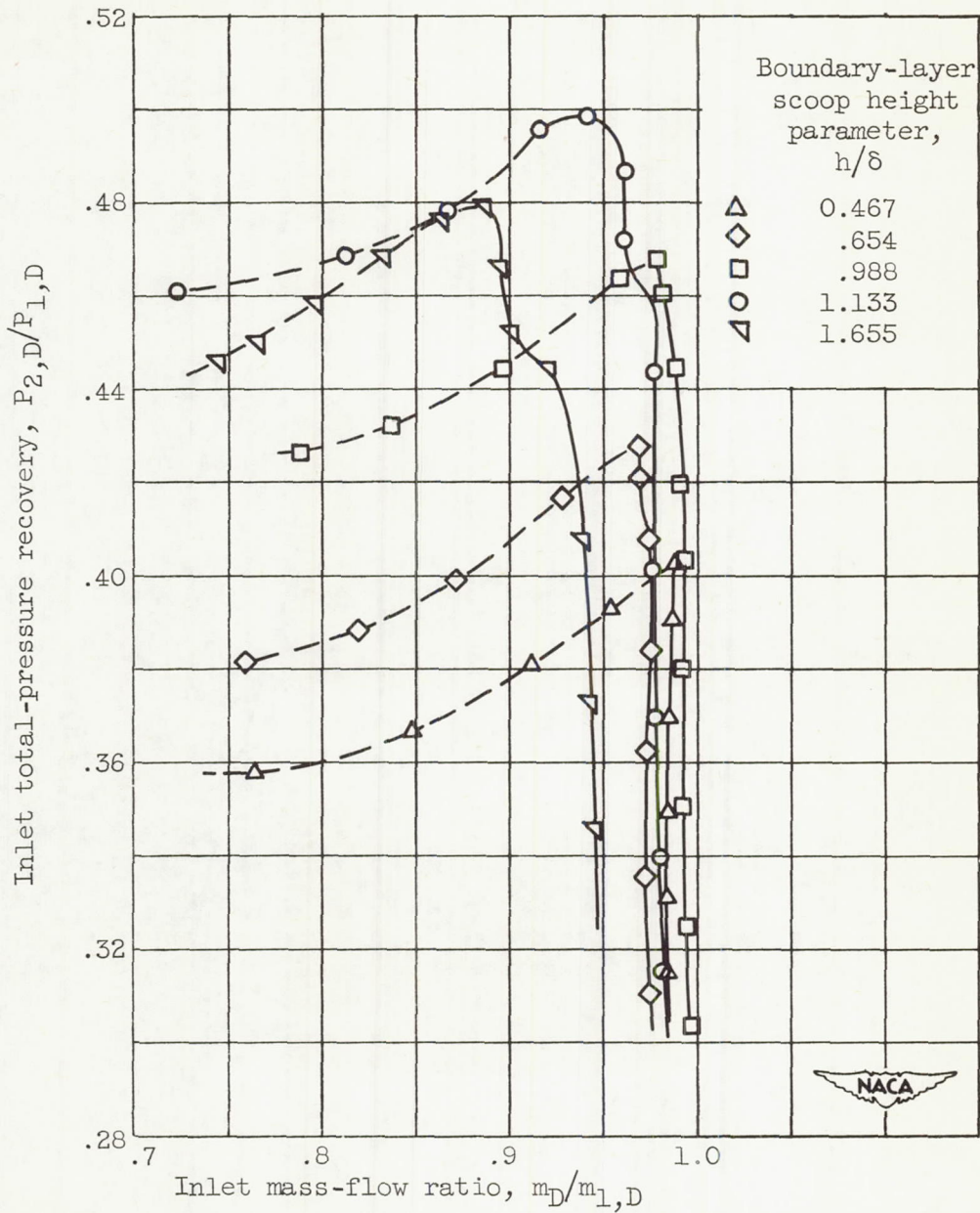
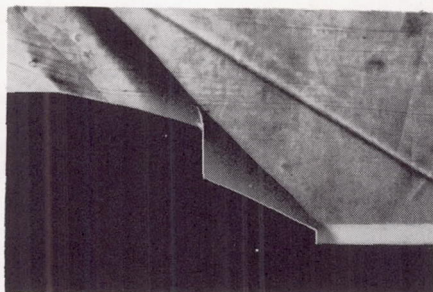
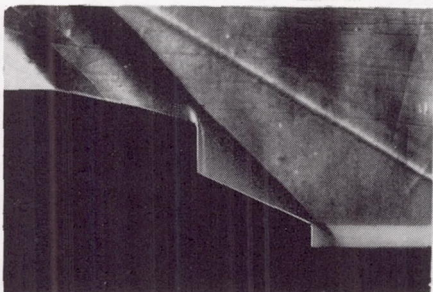


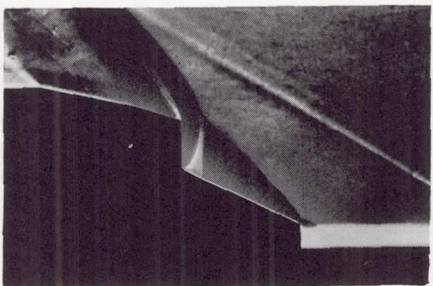
Figure 16. - Effect of wedge boundary-layer removal on inlet pressure recovery and mass flow at Mach 2.93.



(a)  $h/\delta$ , 0.689;  $P_{2,D}/P_{1,D}$ , 0.756;  
 $m_D/m_{1,D}$ , 0.945.



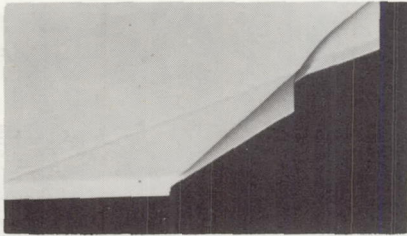
(b)  $h/\delta$ , 1.048;  $P_{2,D}/P_{1,D}$ , 0.811;  
 $m_D/m_{1,D}$ , 0.947.



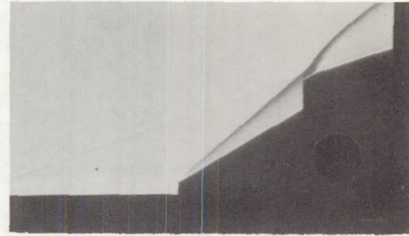
(c)  $h/\delta$ , 1.413;  $P_{2,D}/P_{1,D}$ , 0.877;  
 $m_D/m_{1,D}$ , 0.868.

NACA  
 C-33033

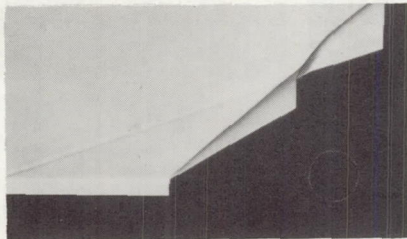
Figure 17. - Steady schlieren photographs of peak pressure conditions for wedge model at Mach 1.88.



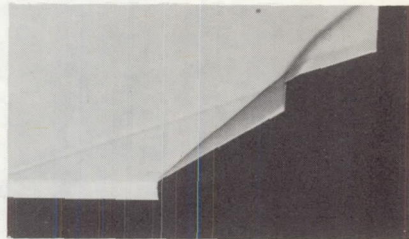
(a)  $h/\delta$ , 0.467;  $P_{2,D}/P_{1,D}$ , 0.403;  
 $m_D/m_{1,D}$ , 0.992.



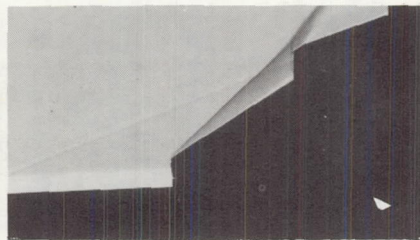
(b)  $h/\delta$ , 0.654;  $P_{2,D}/P_{1,D}$ , 0.428;  
 $m_D/m_{1,D}$ , 0.969.



(c)  $h/\delta$ , 0.988;  $P_{2,D}/P_{1,D}$ , 0.468;  
 $m_D/m_{1,D}$ , 0.978.



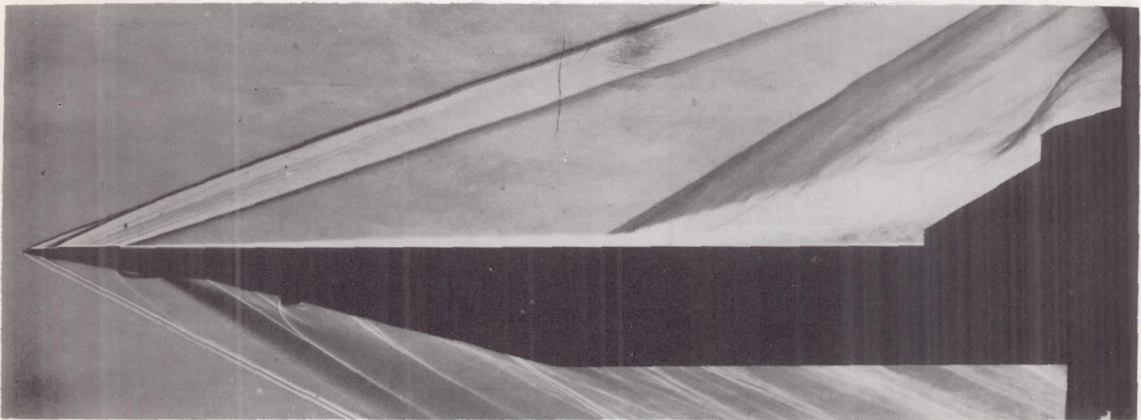
(d)  $h/\delta$ , 1.133;  $P_{2,D}/P_{1,D}$ , 0.498;  
 $m_D/m_{1,D}$ , 0.942.



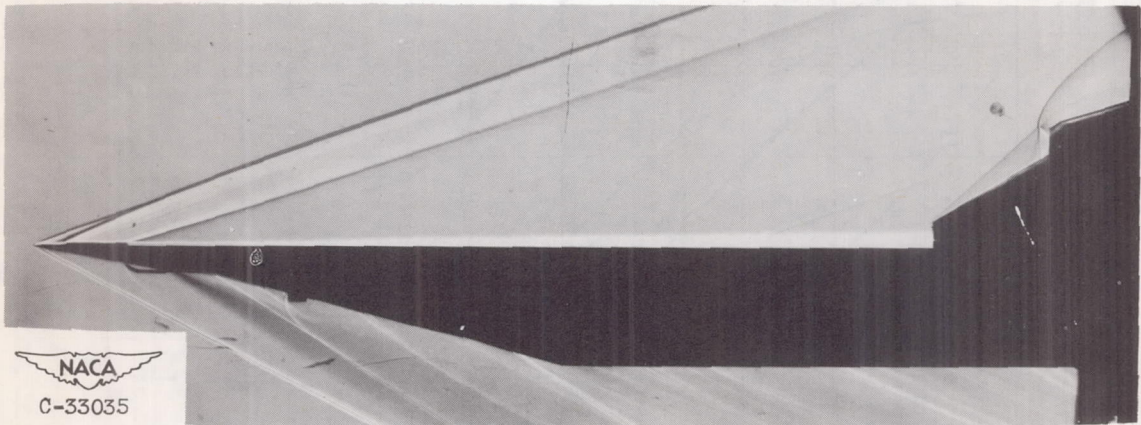
(e)  $h/\delta$ , 1.655;  $P_{2,D}/P_{1,D}$ , 0.479;  
 $m_D/m_{1,D}$ , 0.886.

NACA  
 C-33034

Figure 18. - Steady schlieren photographs of peak pressure conditions for wedge model at Mach 2.93.



(a)  $h/\delta$ , 0.988; average  $P_{2,D}/P_{1,D}$ , 0.432; average  $m_D/m_{1,D}$ , 0.888.



(b)  $h/\delta$ , 1.655; average  $P_{2,D}/P_{1,D}$ , 0.468; average  $m_D/m_{1,D}$ , 0.833.

Figure 19. - Schlieren photographs of wedge model during unsteady operation at Mach 2.93.

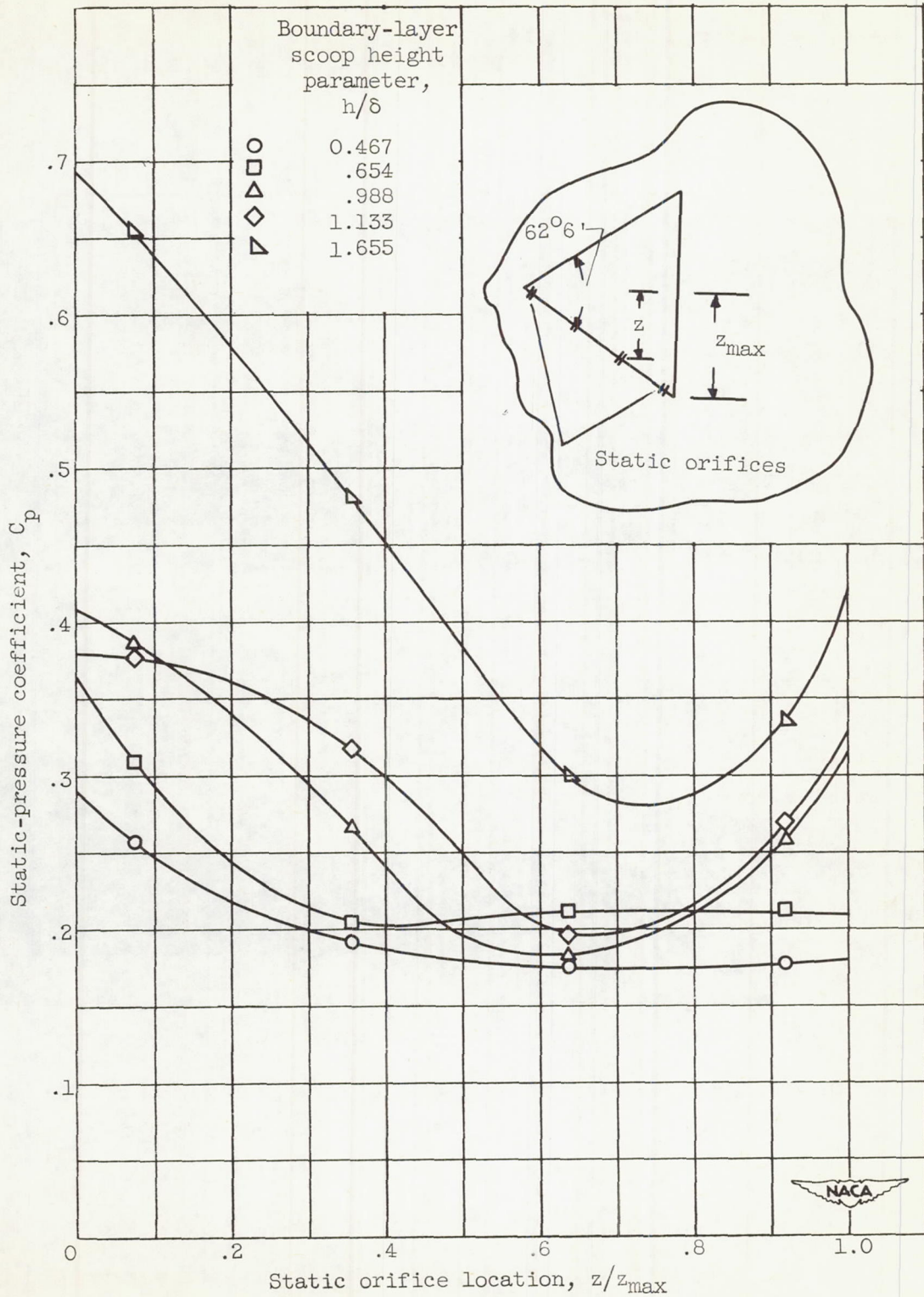


Figure 20. - Wedge static-pressure distributions with supercritical inlet operation at Mach 2.93.

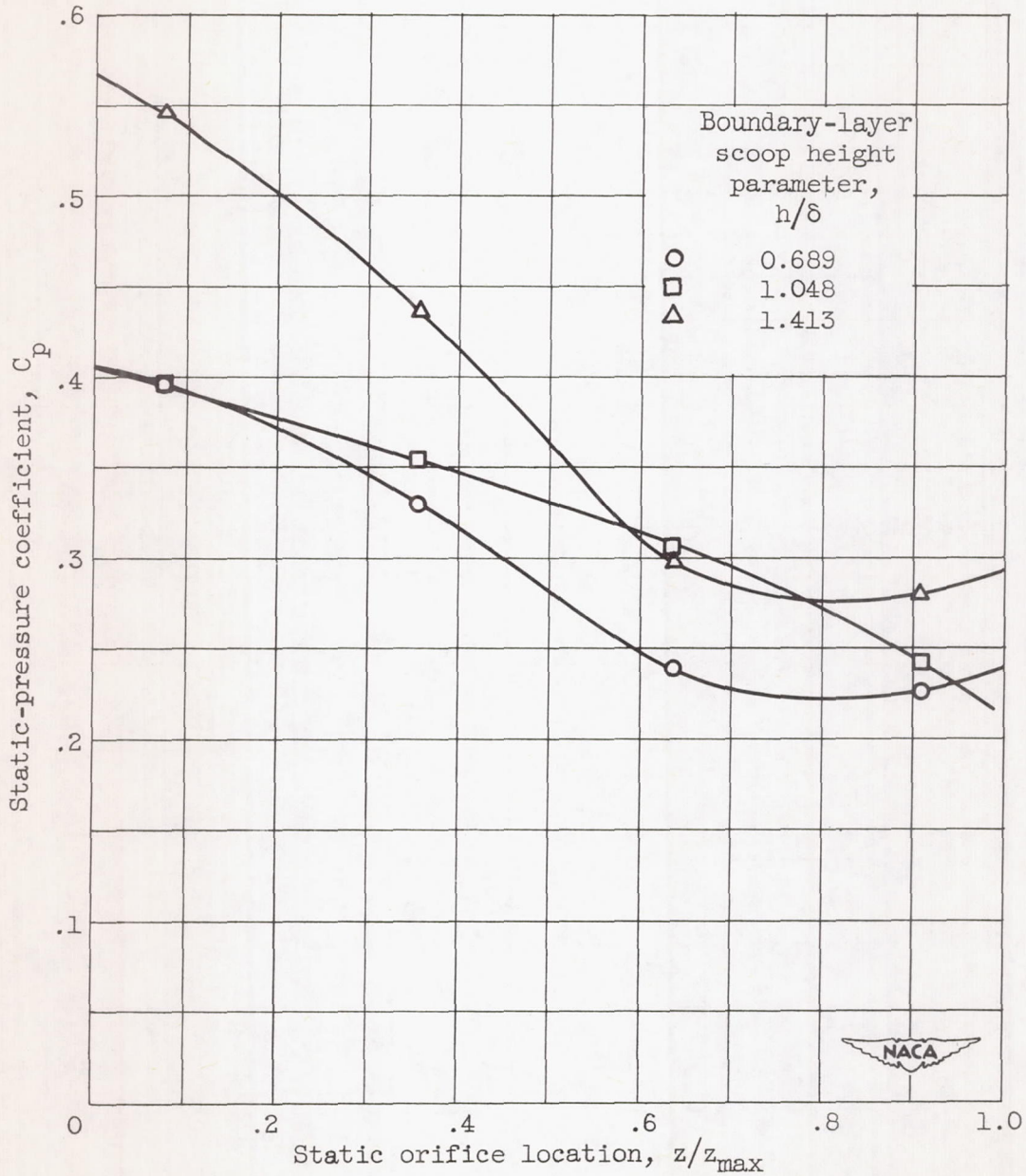


Figure 21. - Wedge static-pressure distributions with supercritical inlet operation at Mach 1.88.

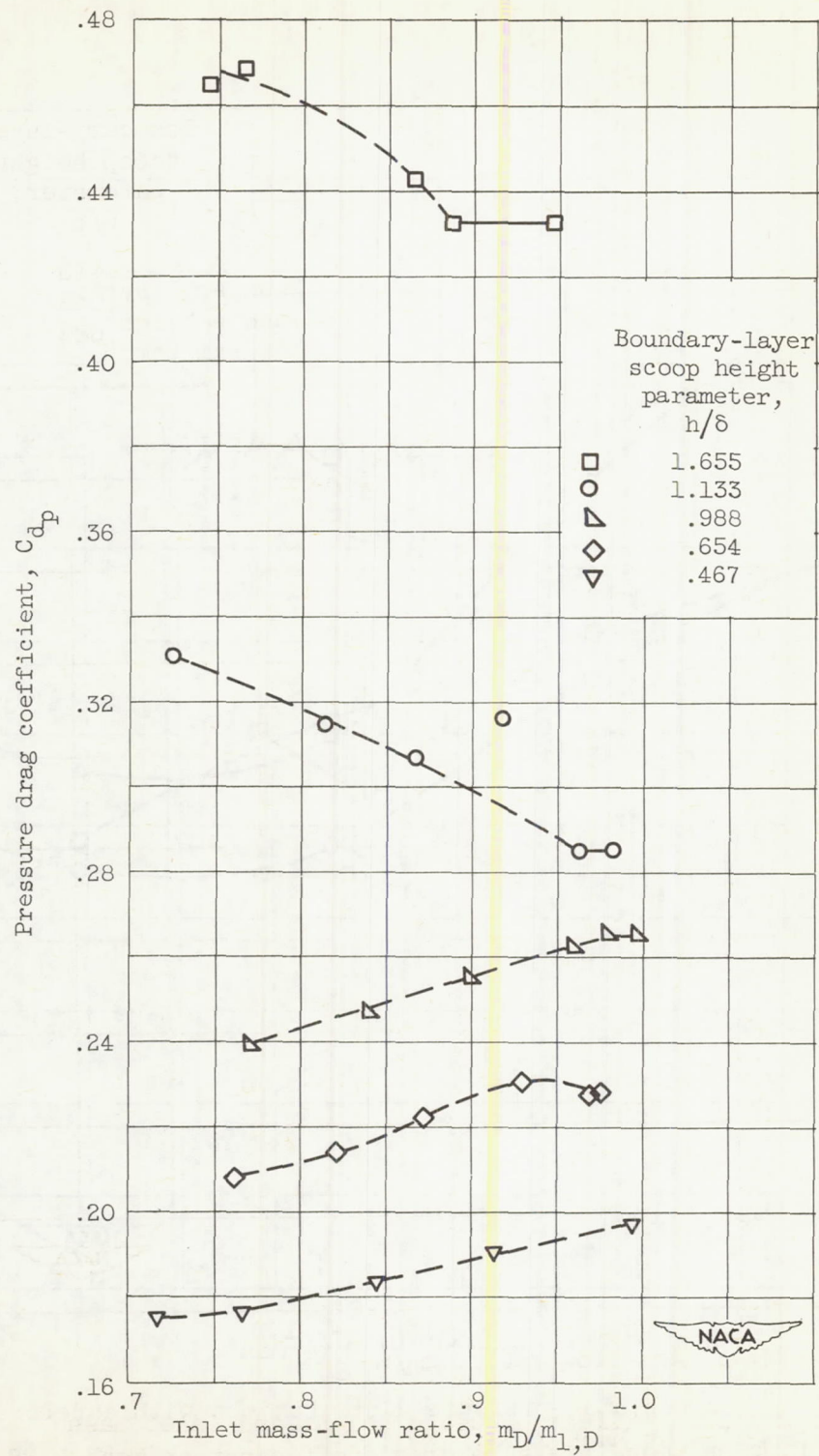


Figure 22. - Effect of wedge height and inlet mass flow on wedge pressure drag coefficient at Mach 2.93.



2944

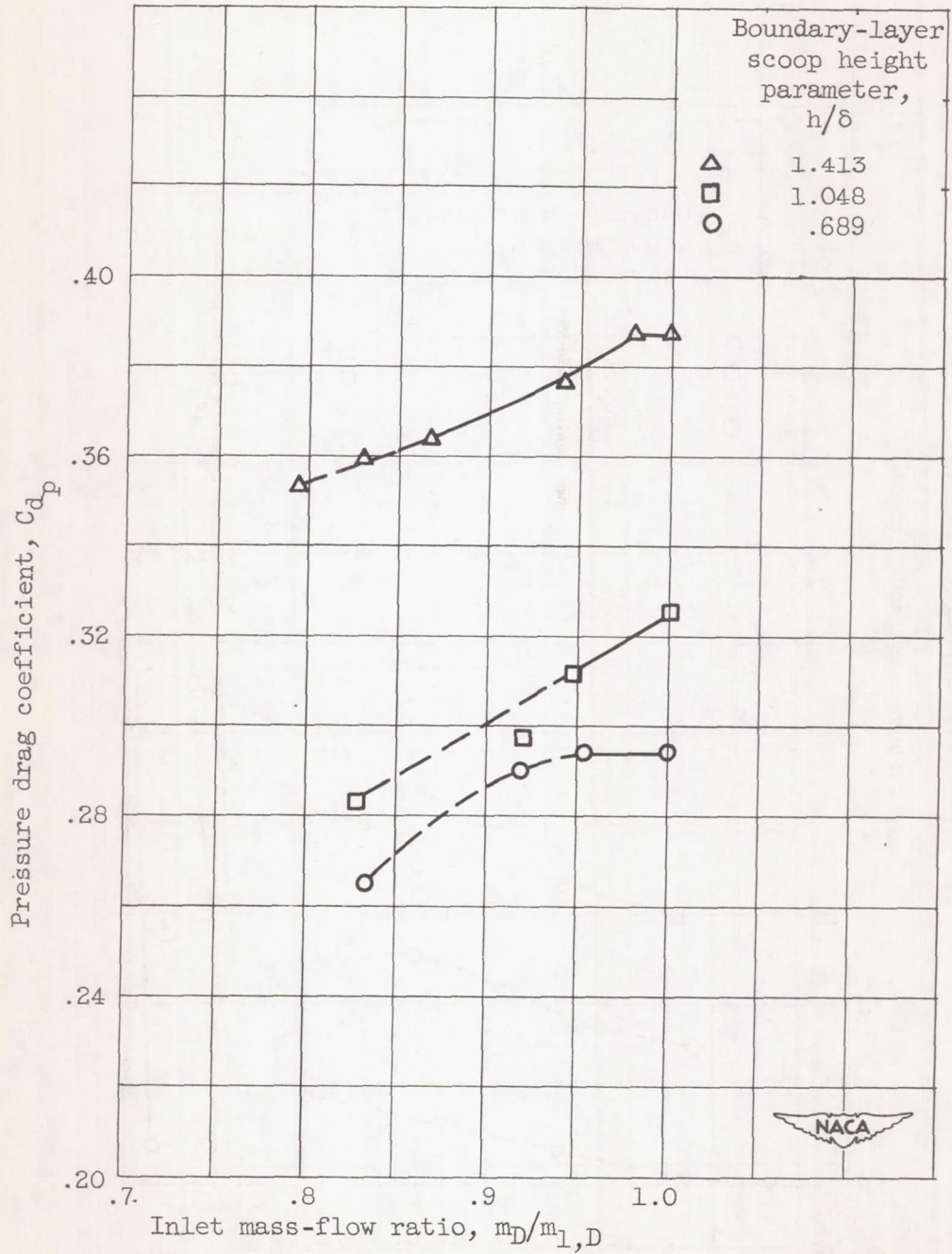


Figure 23. - Effect of wedge height and inlet mass flow on wedge pressure drag coefficient at Mach 1.88.

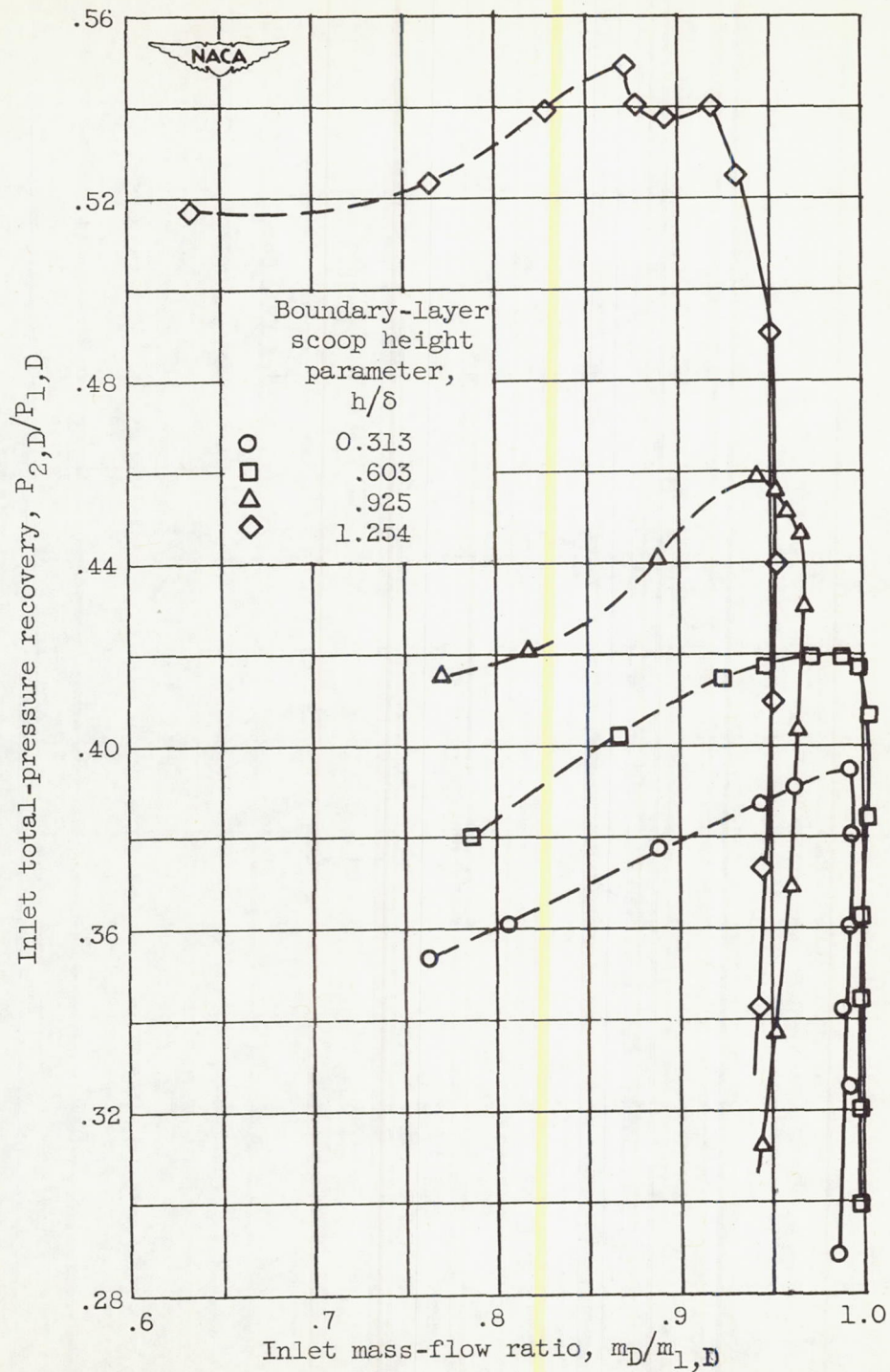
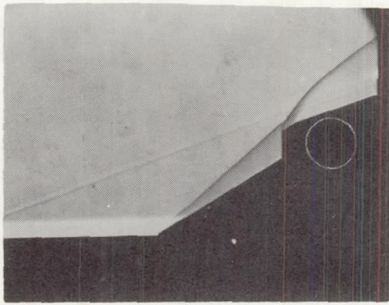


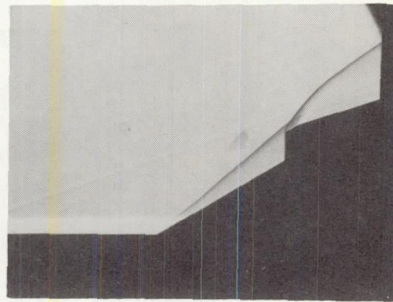
Figure 24. - Effect of cowl lip scoop boundary-layer removal on inlet pressure recovery and mass flow at Mach 2.93.



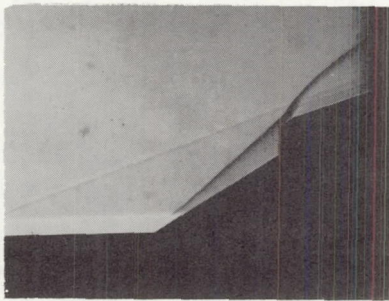
Figure 25. - Effect of cowl-lip scoop boundary-layer removal on inlet pressure recovery and mass flow at Mach 1.88.



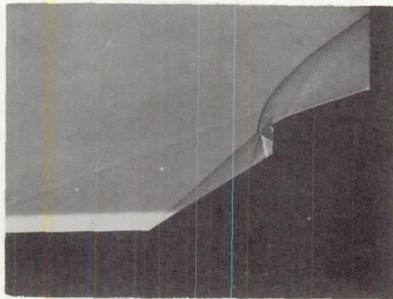
(a)  $h/\delta$ , 0.313;  $P_{2,D}/P_{1,D}$ , 0.395;  
 $m_D/m_{1,D}$ , 0.992.



(b)  $h/\delta$ , 0.603;  $P_{2,D}/P_{1,D}$ , 0.420;  
 $m_D/m_{1,D}$ , 0.988.



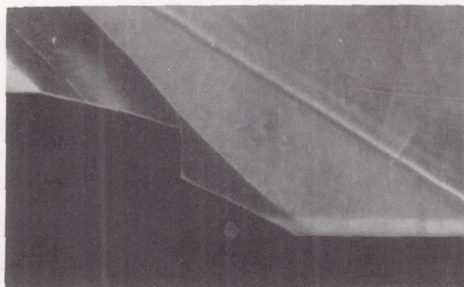
(c)  $h/\delta$ , 0.925;  $P_{2,D}/P_{1,D}$ , 0.459;  
 $m_D/m_{1,D}$ , 0.942.



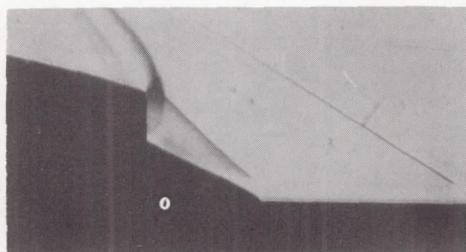
(d)  $h/\delta$ , 1.254;  $P_{2,D}/P_{1,D}$ , 0.549;  
 $m_D/m_{1,D}$ , 0.872.

NACA  
 C-33036

Figure 26. - Schlieren photographs of peak pressure conditions for cowl-lip scoop model at Mach 2.93.



(a)  $h/\delta$ , 1.00;  $P_{2,D}/P_{1,D}$ , 0.826;  
 $m_D/m_{1,D}$ , 0.944. ✓



(b)  $h/\delta$ , 1.361;  $P_{2,D}/P_{1,D}$ , 0.944;  
 $m_D/m_{1,D}$ , 0.642.

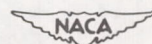
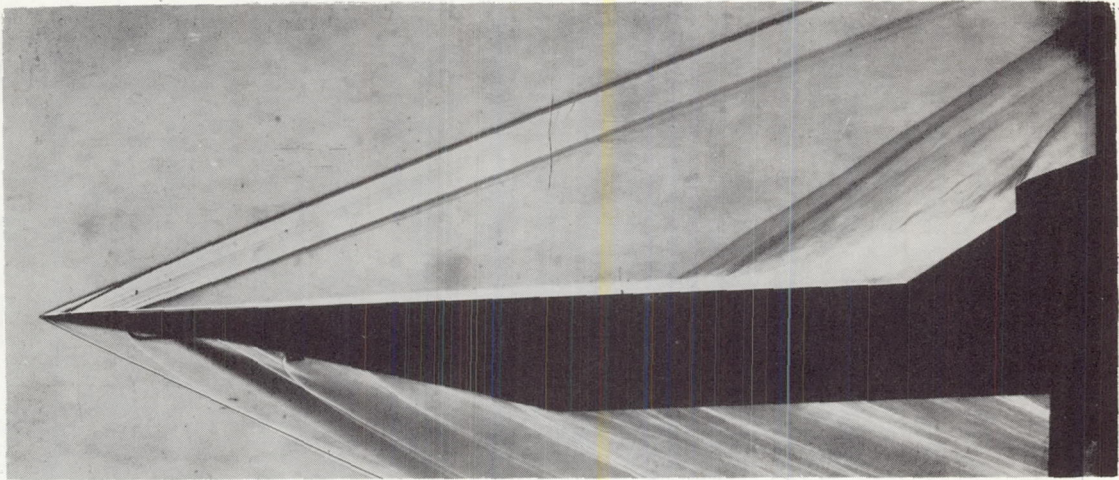
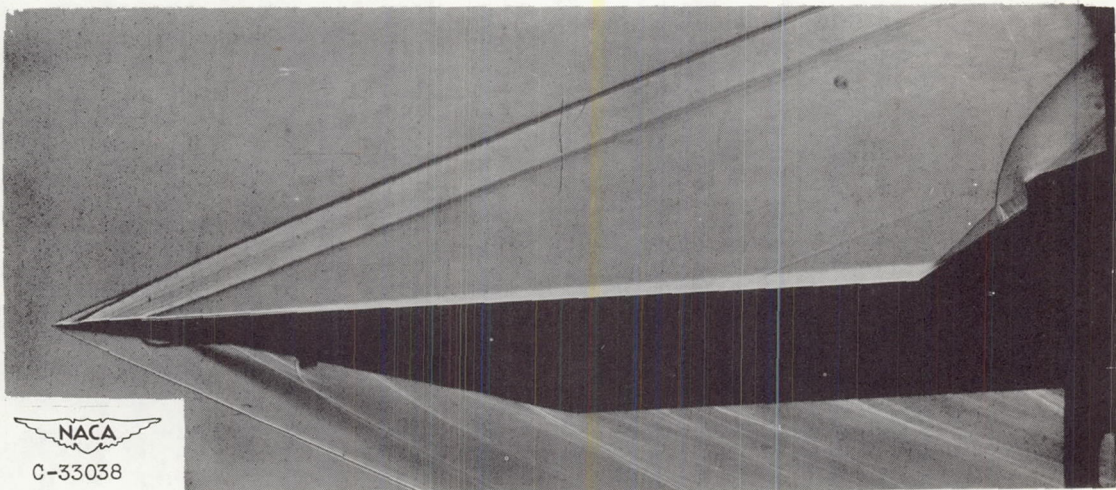
  
C-33037

Figure 27. - Schlieren photographs of peak pressure conditions for cowl-lip scoop model at Mach 1.88.



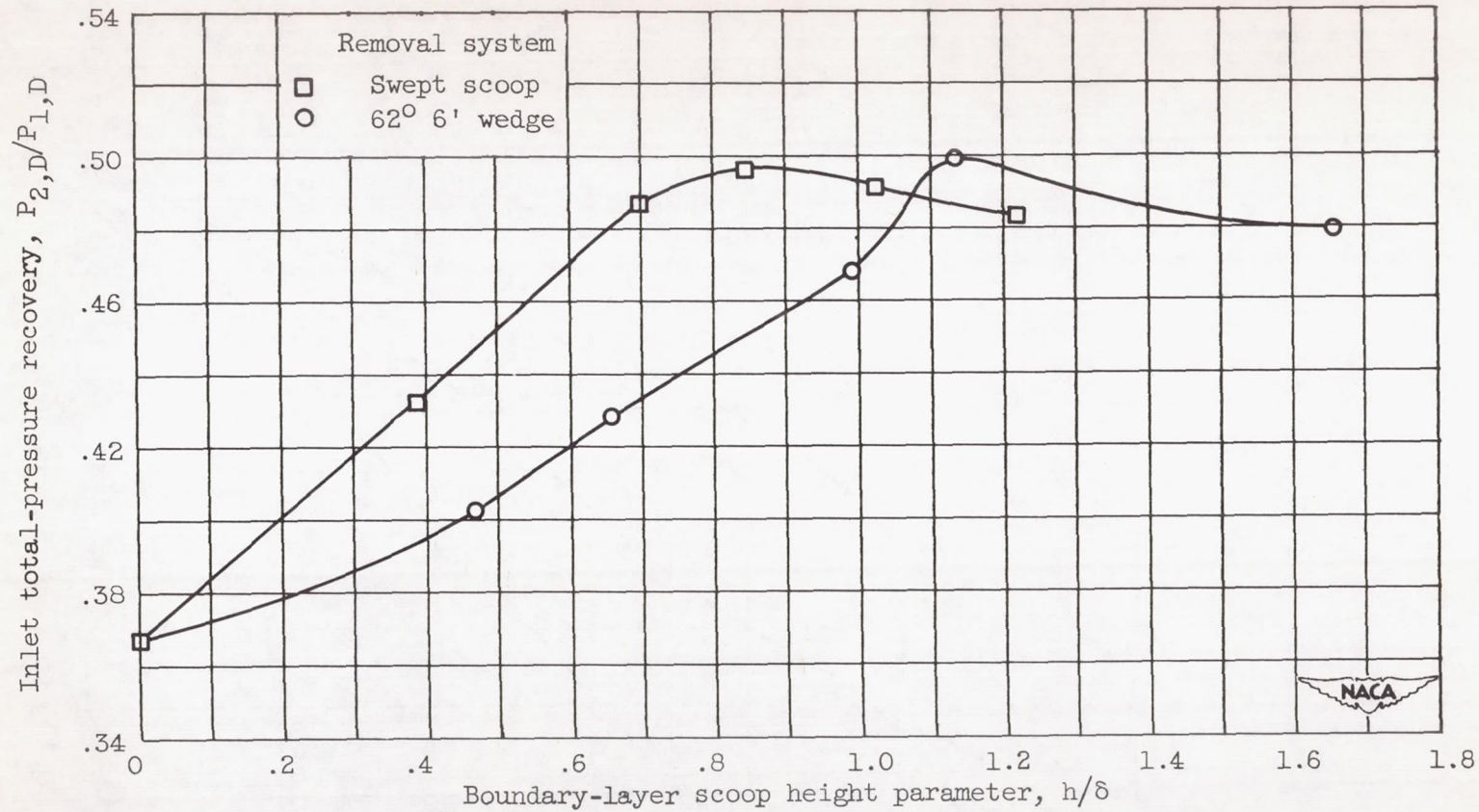
(a)  $h/\delta$ , 0.925; average  $P_{2,D}/P_{1,D}$ , 0.421; average  $m_D/m_{1,D}$ , 0.816.



NACA  
C-33038

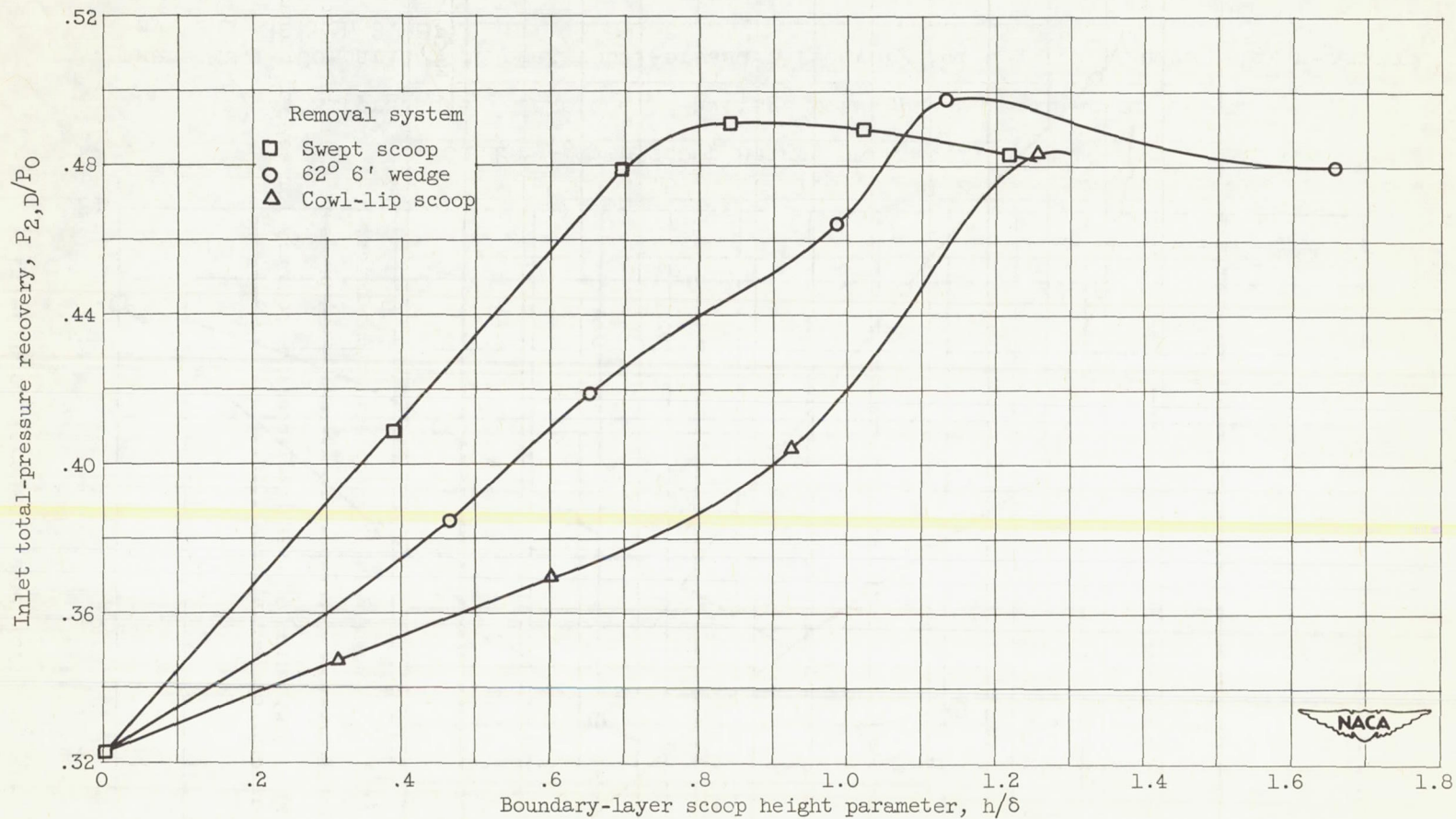
(b)  $h/\delta$ , 1.254; average  $P_{2,D}/P_{1,D}$ , 0.523; average  $m_D/m_{1,D}$ , 0.765.

Figure 28. - Schlieren photographs of cowl-lip scoop removal system during unsteady operation at Mach 2.93.



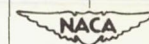
(a) Total pressure referenced to average total pressure ahead of inlet.

Figure 29. - Comparison of peak total-pressure recovery for several boundary-layer-removal systems at Mach 2.93.

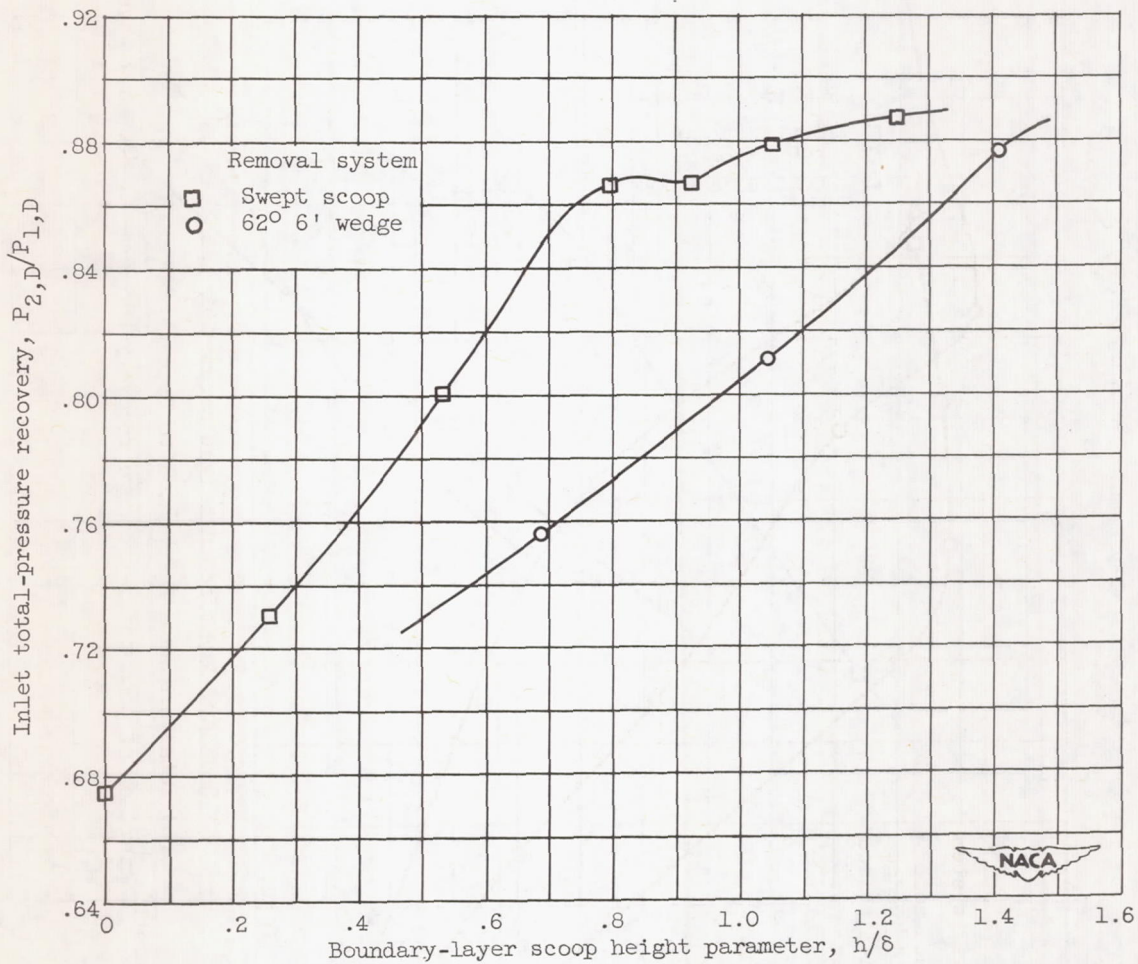


(b) Total pressure referenced to free-stream value.

Figure 29. - Concluded. Comparison of peak total-pressure recovery for several boundary-layer-removal systems at Mach 2.93.

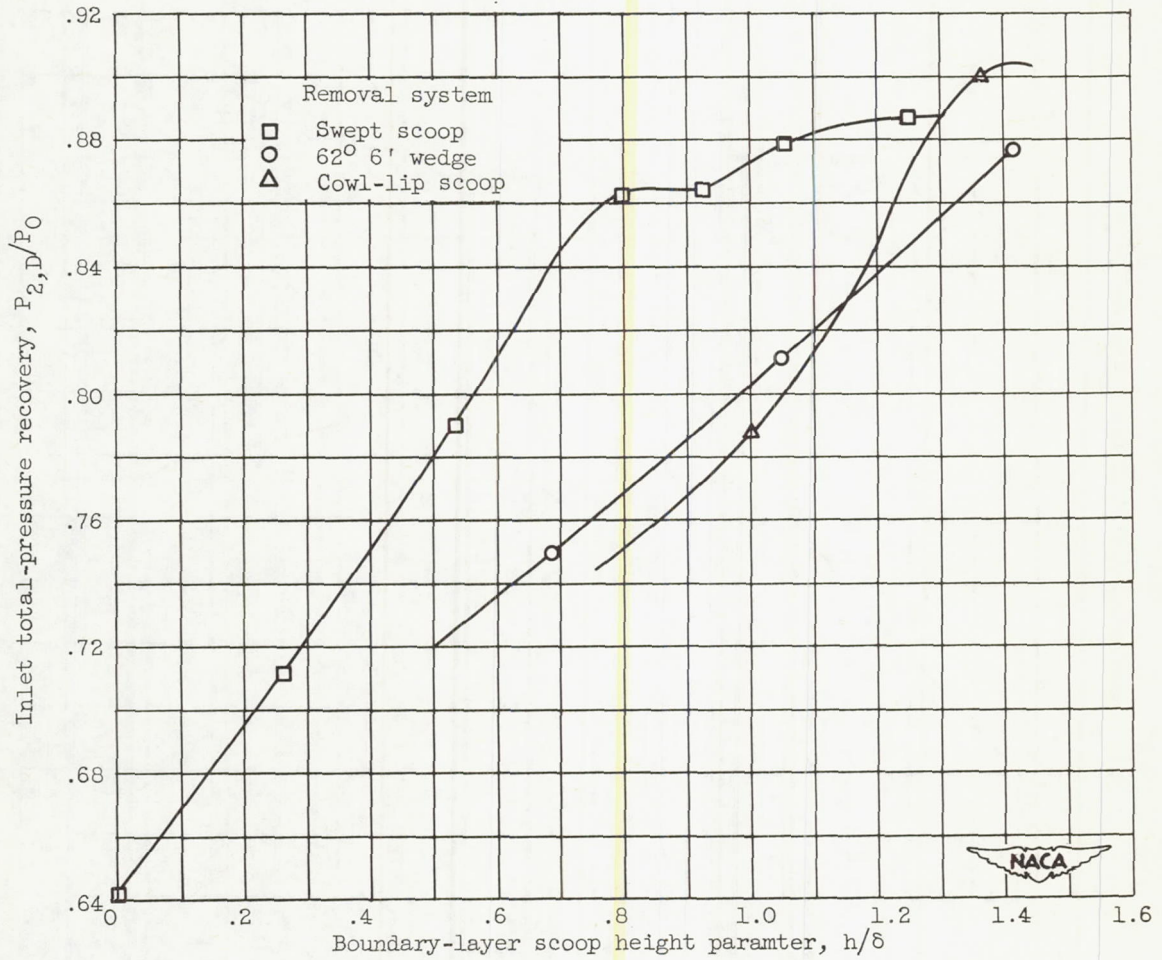






(a) Total pressure referenced to average total pressure ahead of inlet.

Figure 30. - Comparison of peak total-pressure recovery for several boundary-layer-removal systems at Mach 1.88.



(b) Total pressure referenced to free-stream value.

Figure 30. - Concluded. Comparison of peak total-pressure recovery for several boundary-layer-removal systems at Mach 1.88.

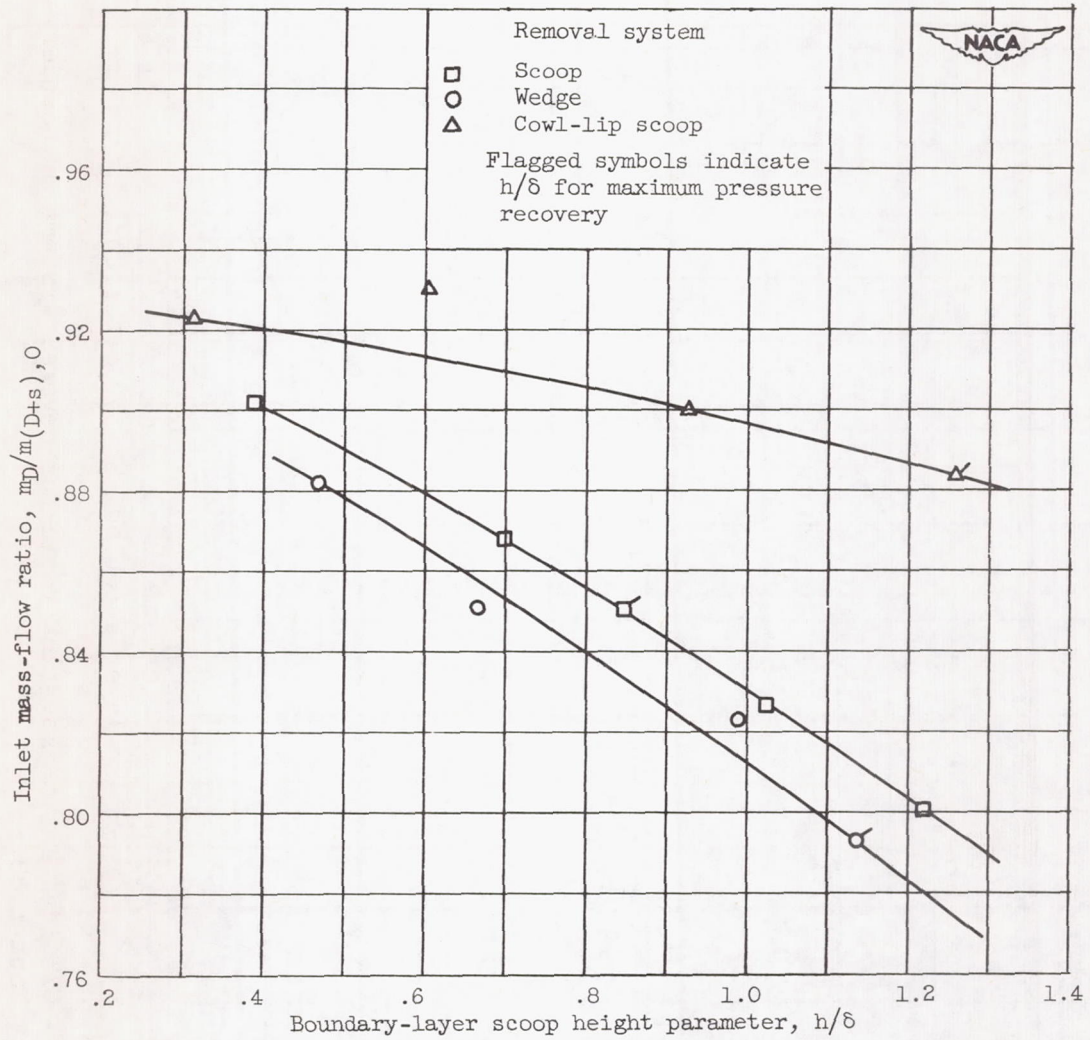


Figure 31. - Critical inlet mass-flow ratio for several systems of boundary-layer removal at Mach 2.93.

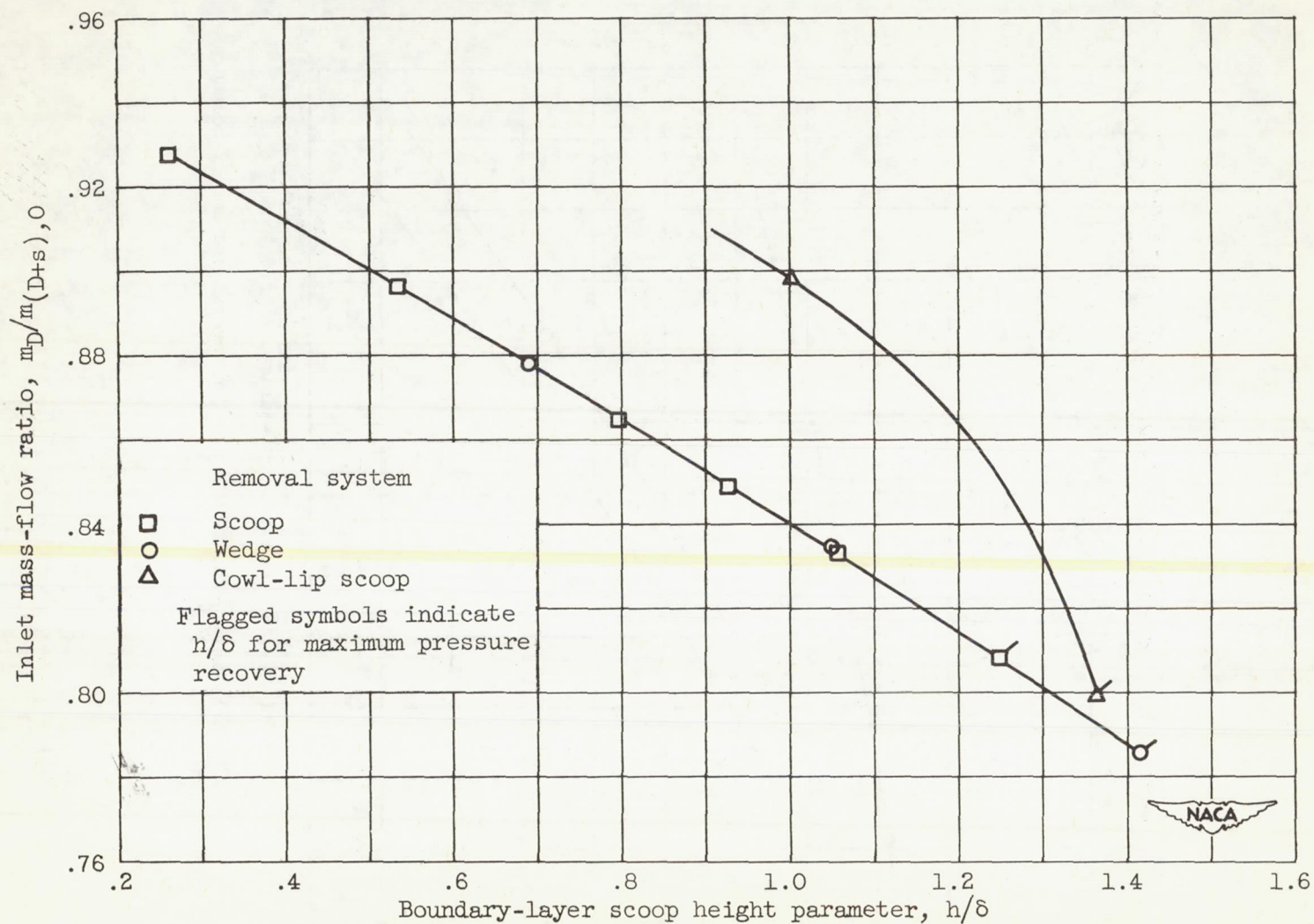


Figure 32. - Critical inlet mass-flow ratio for several systems of boundary-layer removal at Mach 1.88.

1. The first part of the paper is devoted to the study of the properties of the function  $f(x)$  defined by the equation  $f(x) = \int_0^x f(t) dt$ . It is shown that  $f(x)$  is a constant function.

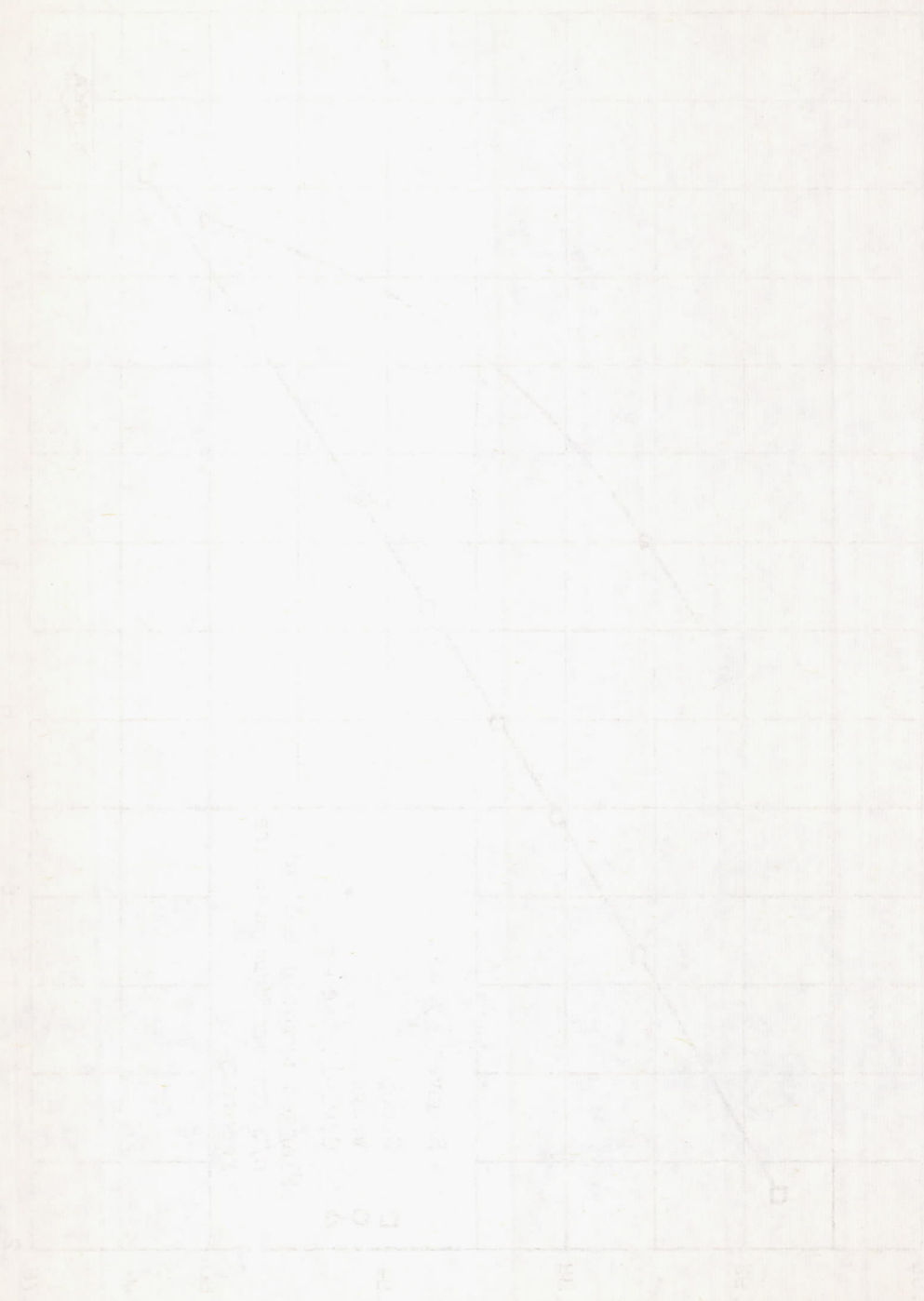


Figure 1. Graph of the function  $f(x) = \int_0^x f(t) dt$ .

